Torsional Vibration and stability Analysis by Bond Graph Modelling: A practical approach, part two.

Tjeerd Heeringa BSc, EEng, M IMarEST, M ASME, M IEEE*, Israel Núñez-Hernández MSc[a]

[a]TMC, The Netherlands
* Corresponding author. Email: t.heeringa@heeringa-engineering.com

Synopsis

The traditional modelling approach in engineering is mathematical, but thanks to the advances in computer technology it is now possible for the practical engineer to model physical systems in a more "user friendly" way.
This paper will demonstrate the power and simplicity of Bond Graphs in modelling technique. Bond Graph modelling was original developed in the late 1950s by the late Professor Henry M. Paynter of MIT. Professor Paynter acted well before his time as the main advantage of his creation, other than the modeling insight that it provides and the ability of effectively dealing with mechatronics, came into fruition only with the recent advent of modern computer technology and the tools derived as a result of it, including symbolic manipulation, MATLAB and SIMULINK and the simulation package 20-sim, which allows direct input of the Bond Graph.

Keywords: Electro-mechanical vibrations, Bond Graph modelling, Park equation, Maxwell element.

1. Introduction

This paper is a continuation of a paper presented at the INEC 2018 [48] which showed a practical modelling approach of parallel running generator sets as used in ship's system for power generation.

A practical generator model for use in torsional vibration analysis was presented in the INEC 2018 paper, in this paper we will present a 3-phase generator model using the Bond Graph method. For observing high frequency events and the effect of the rectifier load to the generator and the dynamics or stability of parallel switching of generator set's we need a more detailed generator model.

The Bond Graph technic was explained in the INEC 2018 paper [49] and will not repeated here. As in the authors view in most literature the description of the synchronous generator is not very readable for the practical engineer this paper will start with an explanation of the synchronous machine following the book of Kundur and clarify some of the formulae presented in Kundur's book.

The synchronous machine is a complex rotating mass-spring system and the swing equation is extensive discussed in the 2018 paper and will also not repeated here. The flexible coupling between the prime mover and the generator will also reviewed, it appears to be a highly nonlinear piece of equipment. An attempt was made to develop a practical model of the rubber element based on the measurements at the VULKAN premises during a FAT. Most models in literature are based on physics, the model in this paper will be measurement based.

For a more thoroughly analysis of bond graphs the author refer to the extensive amount of literature available see among others the reference list: [1], [4], [5], [6], [9], [10], [12], [13], [14], [15], [16], [17], [19], [20]. Reference [40] and [42] gives a particularly good introduction in the use of bond graphs. Reference [41] is an example how to use bond graphs in electronics. Finally, for MATLAB users there is Bond graph add-on block library BG V2.1. see www.mathworks.com.

Author's Biographies
Tjeerd Heeringa is currently working as a consultant in control engineering problem solving by simulations after his retirement. Before his retirement working in several positions as a senior superintend of Boskalis dredging
Israel Núñez-Hernández is working at imec The Netherlands via TMC. He is writing his PhD thesis (University of Twente) on modelling and simulation of electrical machines by means of the port-based approach.

2. The Synchronous Machine.

We like to start with a description of the two-pole synchronous machine as depicted in Figure 1. The three stator windings with the three stator voltages u_a, u_b, and u_c. The rotor excitation and a damper winding are on the d-axis, and another damper winding on the q-axis.
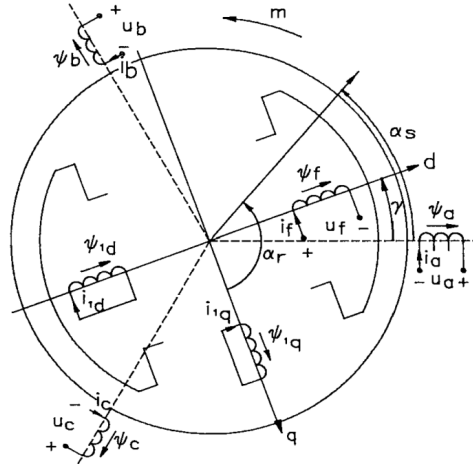

Figure 1: Salient-pole synchronous machine.

For this document we assume:
- The inside of the stator surface is smooth, the effects of the winding slots are neglected
- Hysteresis, eddy current, (and skin-effect) and saturation phenomena are neglected.
- Between the reference direction off current and flux there is the same connection as between the direction of turning and the forward movement of a right screw.
- The magnetic circuit of the rotor is symmetrical with reverence to the d- and q axis
- The excitation winding, which axis is on the d-axis, is the only winding on the rotor which has access. Next to it there is a damper winding on the d-axis (salient rotor) and a round rotor has also a damper winding in the q-axis.

The stator windings are placed in a sinus form way along the stator outline:

$$Z_a(\alpha_s) = \hat{Z} \sin(\alpha_s)$$
$$Z_b(\alpha_s) = \hat{Z} \sin\left(\alpha_s - \tfrac{2}{3}\pi\right)$$
$$Z_c(\alpha_s) = \hat{Z} \sin\left(\alpha_s + \tfrac{2}{3}\pi\right)$$

where Z is the amount of wires per meter and $\hat{Z}$ is the maximum.
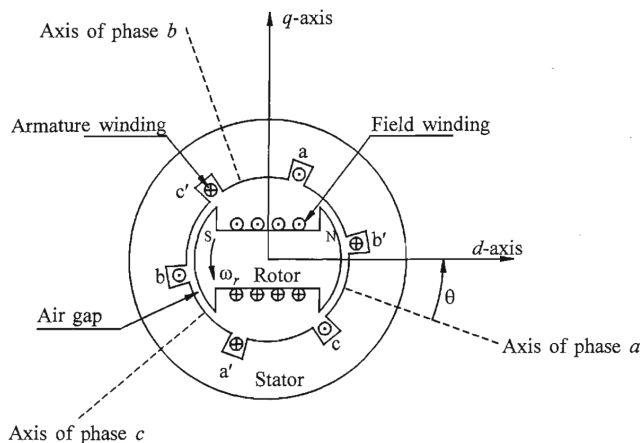

Figure 2: Schematic diagram of a three-phase synchronous machine [27].

The three-phase windings of the armature are distributed 120º apart in space so that, with uniform rotation of the magnetic rotor field, voltages displaced by 120º in time phase will be produced in the windings. When carrying balanced three-phase currents (motor) the armature will produce a magnetic field in the air gap rotating at synchronous speed. The field produced by the direct current in the rotor winding, revolves with the rotor. For production of a steady torque the fields of stator and rotor must rotate at the same speed.

There are two basic structures used, depending on speed. For low speeds (about 1000 rpm) a rotor with salient or projecting poles and concentrated windings are used. Such rotors often have damper windings in the form of copper rods embedded in the pole face as shown in Figure 3.
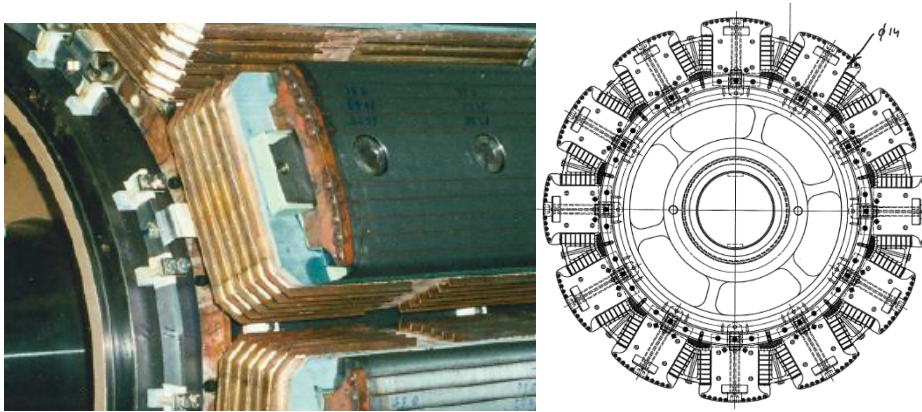

Figure 3: Salient pole rotor of a 11.35 MVA 5500 V 500 rpm generator, drawing and rotor pole picture.

On the other hand, for high speed (steam and gas turbines) there generators have round, or cylindrical rotors made up of solid steel forgings as shown in Figure 4.
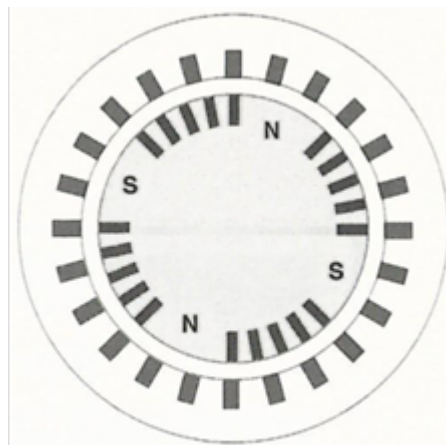

Figure 4: Example of a round rotor machine.

Machines with more than one pair of field poles will have stator windings made up of a corresponding multiple set of coils. For purposes of analysis, it is convenient to consider only a single pair of poles and recognize that conditions associated with other pole pairs are identical to those for the pair under consideration.

Therefore, angles are normally measured in electrical radians or degrees. The angle covered by one pole pair is 2π radians or 360 electrical degrees.

2.1. MMF Waveforms.

In practice, the armature windings and round rotor machine field windings are distributed in many slots so that the resulting mmf and flux waveforms have nearly sinusoidal space distribution. In the case of salient pole machines, which have field windings concentrated at the poles, shaping of the pole faces is used to minimize harmonics in the flux produced.

First, let us consider the mmf waveform due to the armature windings only. The mmf produced by current flowing in only one coil in phase a is illustrated in Figure 5, in which the cross section has been cut open and rolled out in order to develop a view of the mmf wave.
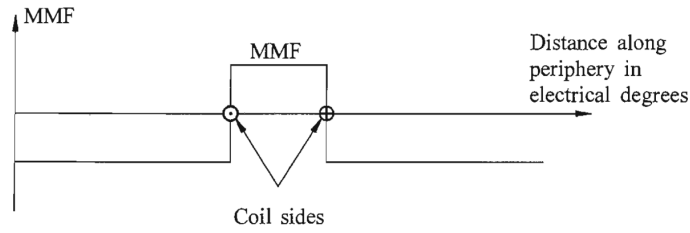
Figure 5: MMF waveform due to a single coil.

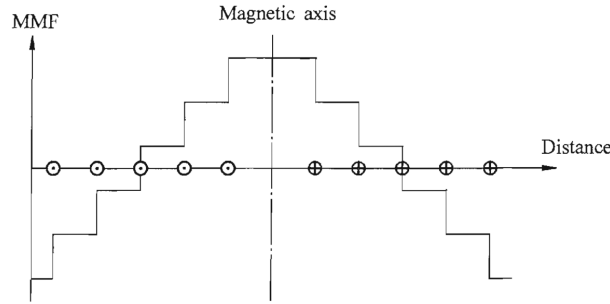By adding more coils, the mmf wave distribution shown in Figure 6 may be obtained.

Figure 6: MMF waveform due to a number of coils.

We see the mmf waveform is progressing from a square wave toward a sine wave as coils are added. Machine design aims at minimizing harmonics. For most analyses of machine performance, it is reasonable to assume that each phase winding produces a sinusoidally distributed mmf wave. The windings are then said to be sinusoidally distributed. The harmonics may be considered as secondary from the viewpoint of machine performance. In addition to causing rotor surface eddy current losses, harmonics contribute to armature leakage reactances.

2.2. Rotating magnetic field

Let us now determine the net mmf wave due to the three-phase windings in the stator. Figure 6 shows the mmf wave of phase a.
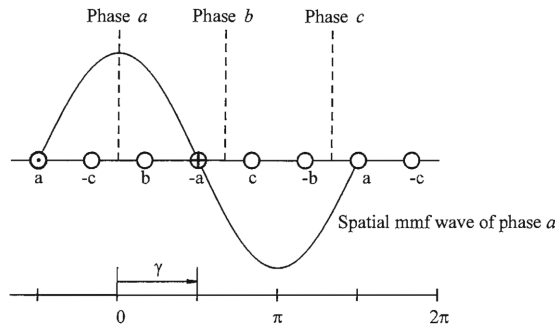

Figure 7: Spatial mmf wave of phase a

With γ representing the angle along the periphery of the stator with respect to the center of phase a, the mmf wave due to the three phases may be described as follows:

$$MMF_a = Ki_a \cos \gamma \tag{2.1}$$

$$MMF_b = Ki_b \cos\left(\gamma - \frac{2}{3}\pi\right) \tag{2.2}$$

$$MMF_b = Ki_b \cos\left(\gamma + \frac{2}{3}\pi\right) \tag{2.3}$$

where i_a, i_b and i_c are the instantaneous values of the phase currents and K is a constant. Each winding produces a stationary mmf wave whose magnitude changes as the instantaneous value of the current through the windings change. The three mmf waves due to the three phases are displayed 120 electrical degrees apart in space. With balanced phase currents, and time origin arbitrarily chosen as the instant when i_a is maximum, we have:

$$i_a = I_m \cos(\omega_s t) \tag{2.4}$$

$$i_b = I_m \cos\left(\omega_s t - \frac{2}{3}\pi\right) \tag{2.5}$$

$$i_c = I_m \cos\left(\omega_s t + \frac{2}{3}\pi\right) \tag{2.6}$$

where $\omega_s = 2\pi f$ is the angular frequency of stator currents in electrical rad/s. The total mmf due to the three phases is given by:

$$MMF_{total} = MMF_a + MMF_b + MMF_c$$
$$= KI_m\left[\cos(\omega_s t)\cos\gamma + \cos\left(\omega_s t - \frac{2\pi}{3}\right)\cos\left(\gamma - \frac{2\pi}{3}\right) + \cos\left(\omega_s t + \frac{2\pi}{3}\right)\cos\left(\gamma + \frac{2\pi}{3}\right)\right] \tag{2.7}$$

See Appendix 2 for the evidence to get from the above expression for the total mmf the expression of a traveling wave:

$$MMF_{total} = \frac{3}{2}KI_m \cos(\omega_s t - \gamma) \tag{2.8}$$

This is the equation of a travelling wave. At any instant of time, the total mmf has a sinusoidal spatial distribution. It has a constant amplitude and a space-phase angle $\omega_s t$, which is a function of time. Thus, the entire mmf wave moves at the constant angular velocity of ω_s electrical rad/s.

For a machine with p_f field poles, the speed of rotation of the stator field is:

$$\omega_m = \frac{2}{p_f}\omega_e \qquad \text{mech. rad/sec} \tag{2.9}$$

or

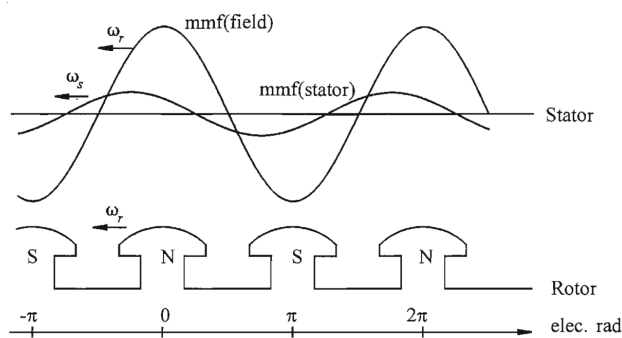$$n = \frac{60}{2\pi}\omega_m = \frac{120}{p_f}f \qquad \text{rev/min} \tag{2.10}$$

Figure 8: Stator and rotor mmf wave shapes [27].

The stator and rotor mmf waves are shown in Figure 8 relative to the rotor structure, again with both stator and rotor cross sections rolled out.

The electromagnetic torque on the rotor acts in a direction so as to bring the magnetic fields into alignment. If the field leads the armature field, the torque acts in opposition to the rotation with the machine acting as a generator.

On the other hand, if the rotor field lags the armature field, the torque acts in the direction of rotation with the machine acting as a motor.

2.3. *Mathematical description of a synchronous machine.*

In developing equations of a synchronous machine the following assumptions are made:
- The stator windings are sinusoidal distributed along the air-gap as far as the mutual effects with the rotor are concerned.
- The stator slots cause no appreciable variation of the rotor inductances with the rotor position.
- Magnetic hysteresis is negligible
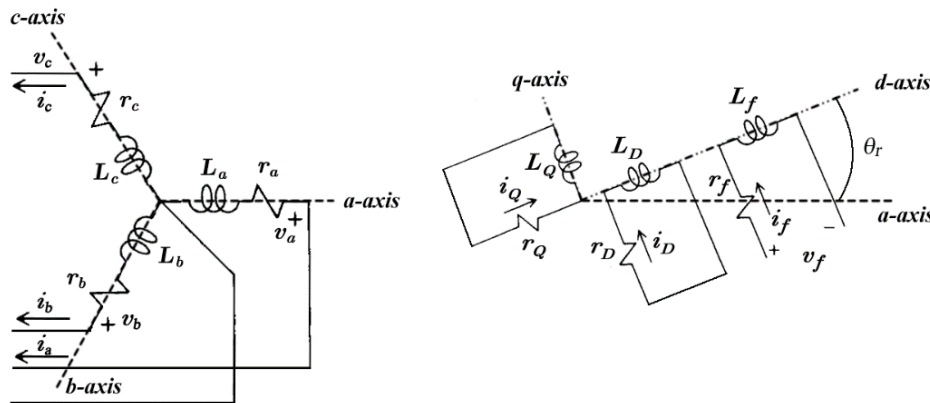- Magnetic saturation effects are negligible

Figure 9: Stator and rotor circuits of a synchronous machine

where the subscripts represent:

a, b, c :   Stator phase windings,

f :   field winding,

D : d-axis amortisseur circuit,

Q : q-axis amortisseur circuit,

θ_r :   angle by which d-axis leads the magnetic axis of phase-a winding, electrical rad.

ω_r :   rotor angular velocity, electrical rad/s

In Figure 2 and Figure 9, θ is defined as the angle by which the d-axis leads the centreline of phase-a winding in the direction of rotation. Since the rotor is rotating with respect to the stator, angle θ is continuously increasing and is related to the rotor angular velocity ω_r and time t as follows:

$$\theta_r = \omega_r t \qquad (2.11)$$

The electrical performance equations of a synchronous machine can be developed by writing equations of the coupled circuits identified in Figure 9.

2.3.1. Basis equations of a Synchronous machine.

We will use the generator convention for polarities so that the positive direction of a stator winding current is assumed to be out of the machine. The positive direction of field amortisseur current is assumed to be into the machine.

In addition to the large number of circuits involved, the fact that the mutual and self-inductances of the stator circuit vary with the rotor position complicates the synchronous machine equations. The variations in inductances are caused by the variations in the permeance of the magnetic flux path due to the non-uniform air-gap. This is pronounced in a salient pole machine in which the permeances in the two axes are significantly different. Even in a round rotor machine there are differences in the two axes due mostly to the large number of slots associated with the field winding.

The flux produced by a stator winding follows a path through the stator iron, across the air-gap, through the rotor iron, back across the air-gap. The variations in permeance of this path as a function of the rotor position can be approximated as:

$$\mathrm{P} = \mathrm{P}_0 + \mathrm{P}_2 \cos 2\alpha \tag{2.12}$$

In the above equation, α is the angular distance from the d-axis along the periphery as shown in Figure 10. A double frequency variation is produced, since the permeances of the north and south poles are equal.
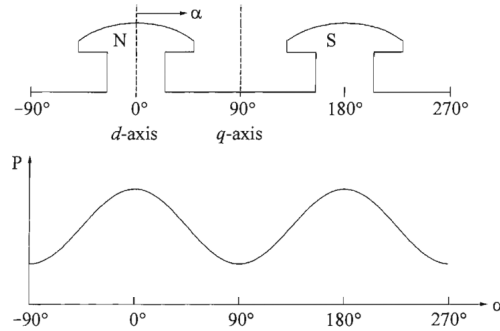

Figure 10: Variation of permeance with rotor position.

We will use the following notation in writing the equations for the stator and rotor circuits:

e_a, e_b, e_c :   instantaneous stator phase to neutral voltages

i_a, i_b, i_c :   instantaneous stator currents in phase a, b, c

e_{fd} :   field voltage

i_f, i_D, i_Q :   field and amortisseur circuit currents

r_f, r_D, r_Q :   rotor circuit resistances

L_a, L_b, L_c :   self-inductances of stator windings

L_{ab}, L_{bc}, L_{ca} :   inductances between stator windings

L_{ad}, L_{aD}, L_{aQ} :   mutual inductances between stator and rotor windings

L_f, l_D, l_Q :   inductances of rotor circuits

r_s :   stator resistance per phase

p :   differential operator d/dt

2.3.2. Stator circuit equations

The voltage equations of the three phases are:

$$e_a = \frac{d\lambda_a}{dt} - r_s = p\psi_a - r_s i_a \tag{2.13}$$

$$e_b = p\lambda_b - r_s i_b \tag{2.14}$$

$$e_c = p\lambda_c - r_s i_c \tag{2.15}$$

The flux linkage in the phase-a winding at any instant is given by:

$$\lambda_a = -L_a i_a - L_{ab} i_b - L_{ac} i_c + L_{af} i_f + L_{aD} i_D + L_{aQ} i_Q \tag{2.16}$$

Similar expressions apply to flux linkages of windings b and c. The units are weber, henrys and amperes. The negative sign associated with the stator winding currents is due to their assumed direction.

As shown below, all the inductances in equation (2.16) are functions of the rotor position and are thus time-varying.

2.3.3. Stator self-inductances

The self-inductance L_a is equal to the ratio of flux linkage phase-a winding to the current i_a, with currents in all other circuits equal to zero. The inductance is directly proportional to the permeance, which as indicated earlier has a second harmonic variation. The inductance L_a will be a maximum for $\theta = 0$, a minimum for $\theta = \pi/2$, a maximum again for $\theta = \pi$, and so on.

Neglecting space harmonics, the mmf of phase-a has a sinusoidal distribution in space with its peak centred on the phase-a axis. The peak amplitude of the mmf wave is equal to $N_a i_a$, where N_a is the effective turns per phase. As shown in Figure 11, this can be resolved into other sinusoidally distributed mmf's, one centered on the d-axis and the other on the q-axis.

The peak values of the two components waves are

$$\text{Peak } MMF_{ad} = N_a i_a \cos\theta \tag{2.17}$$

$$\text{Peak } MMF_{aq} = N_a i_a \cos(\theta + \pi/2) = -N_a i_a \sin\theta \tag{2.18}$$

The reason for resolving the mmf into the d-and q-axis components is that each acts on specific air-gap geometry of defined configuration, Air-gap fluxes per pole along the two axes are

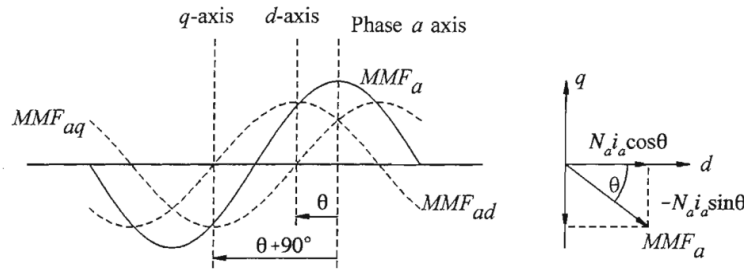

Figure 11: Phase-a mmf wave and its components.

$$\phi_{gad} = (N_a i_a \cos\theta)P_d \tag{2.19}$$

$$\phi_{gaq} = (-N_a i_a \sin\theta)P_q \tag{2.20}$$

In the above, Π_d and Π_q are the permeance coefficients of the d- and q-axis, respectively. In addition to the actual permeance, they include factors required to relate flux per pole with peak value of the mmf wave.

The total air-gap flux linking phase-a is

$$\phi_{gaa} = \phi_{gad} \cos\theta - \phi_{gaq} \sin\theta \tag{2.21}$$

Substituting equations (2.19) and (2.20) in (2.21):

$$\begin{aligned}
\phi_{gaa} &= \cos\theta \left(N_a i_a \cos\theta \right)P_d - \sin\theta(-N_a i_a \sin\theta)P_q \\
&= \left(N_a i_a \cos^2\theta \right)P_d + \left(N_a i_a \sin^2\theta \right)P_q
\end{aligned} \tag{2.22}$$

After some fiddling with trigonometric conversions: a) $\cos 2\alpha = 2\cos^2\alpha - 1$, and b) $\sin^2\alpha = 1 - \cos^2\alpha$, we get:

$$\phi_{gaa} = N_a i_a \left(\frac{P_d + P_q}{2} + \frac{P_d - P_q}{2} \cos 2\theta \right) \tag{2.23}$$

The self-inductance L_a of phase-*a* due to the air-gap flux is:

$$L_a = \frac{N_a}{i_a}\phi_{gaa} = N_a^{\ 2}\left(\frac{P_d + P_q}{2} + \frac{P_d - P_q}{2}\cos 2\theta\right)$$
$$= L_{g0} + L_{aa2}\cos 2\theta_r \tag{2.24}$$

The total self-inductance L_a is given by adding to the above the leakage inductance L_{al} which represents the leakage flux not crossing the air-gap:

$$L_a = L_{al} + L_{gaa}$$
$$= L_{al} + L_{g0} + L_{aa2}\cos 2\theta \tag{2.25}$$
$$= L_{aa0} + L_{aa2}\cos 2\theta$$

Since the windings of phases -*b* and -*c* are identical to that of phase-*a* and are displaced from it by $2\pi/3$ and $4\pi/3$ respectively, we have

$$L_b = L_{aa0} + L_{aa2}\cos 2(\theta - 2\pi/3) \tag{2.26}$$
$$L_c = L_{aa0} + L_{aa2}\cos 2(\theta + 2\pi/3) \tag{2.27}$$

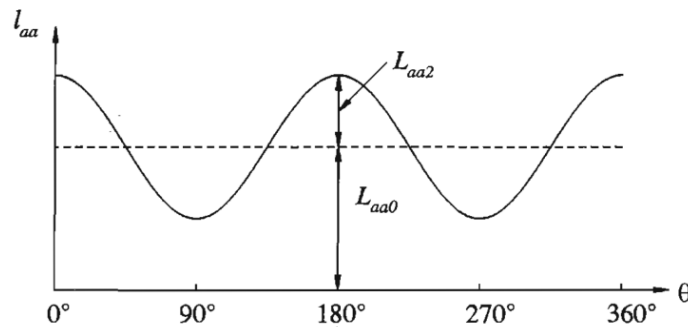The variation of L_a with θ is shown in Figure 13:

Figure 12: Variation of self-inductance of a stator phase.

In equations (2.25) to (2.27) the stator self-inductances have a fixed plus second harmonic terms. Higher order harmonic terms have been neglected.

2.3.4. Stator mutual inductances.

The mutual inductance between two stator windings also exhibits a second harmonic variation because of the rotor shape (salient rotor). It is always negative and has the greatest absolute value when the north and south poles are equidistant from the centers of the two windings concerned. For example, L_{ab} has maximum absolute value when $\theta = -\pi/6$ or $\theta = 5\pi/6$.

The mutual inductance L_{ab} can be found by evaluating the air-gap flux ϕ_{gba} linking phase-*b* when only phase-*a* is excited. As we wish to find the flux linking phase-*b* due to mmf of phase-*a*, θ is replaced by $\theta - 2\pi/3$ in equation (2.23).

$$\phi_{gab} = \phi_{gad}\cos(\theta - 2\pi/3) - \phi_{gaq}\sin(\theta - 2\pi/3)$$
$$= N_a i_a (P_d\cos\theta\cos(\theta - 2\pi/3) + P_q\sin\theta\sin(\theta - 2\pi/3)) \tag{2.28}$$

See the Appendix 3 for further evidence of equations (2.29) to

$$L_{ab} = L_{ba} = \frac{N_a \phi_{gab}}{i_a} = -L_{ab0} + L_{ab2} \cos(2\theta - 2\pi/3)$$
$$= -L_{ab0} - L_{ab2} \cos(2\theta + \pi/3)$$

(2.29)

Similarly,

$$L_{bc} = L_{cb} = -L_{ab0} - L_{ab2} \cos(2\theta - \pi)$$

(2.30)

$$L_{ac} = L_{ca} = -L_{ab0} - L_{ab2} \cos(2\theta - \pi/3)$$

(2.31)

From the above equations, it can be readily seen that $L_{ab2} = L_{aa2}$. This is to be expected since the same variation in permeance produces the second harmonic terms in self and mutual inductances, it can also be seen that L_{ab0} is nearly equal to $L_{aa0}/2$. The variation of mutual inductance between phases a and b as a function of θ is illustrated in figure 14
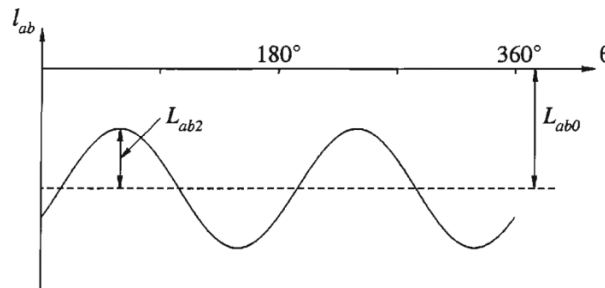

Figure 13: Variation of mutual inductance between stator windings.

2.3.5. Mutual inductance between stator and rotor windings.

With the variations in air-gap due to the stator slots neglected, the rotor circuits see a constant permeance. Therefore, the situation in this case is not one of variation of permeance; instead, the variation in the mutual inductance is due to the relative motion between the windings themselves.

When a stator winding is lined up with a rotor winding, the flux linking the two windings is maximum and the mutual inductance is maximum. When the two windings are displaced by $\pi/2$, no flux links the two circuits and the mutual inductance is zero. With a sinusoidal distribution of mmf and flux waves,

$$L_{af} = L_{af} \cos\theta$$

(2.32)

$$L_{aD} = L_{aD} \cos\theta$$

(2.33)

$$L_{aQ} = -L_{aQ} \sin\theta$$

(2.34)

We now have the expressions for all the inductances that appear in the stator voltage equations. On substituting the expressions for these inductances into equation (2.16), we obtain:

$$
\begin{aligned}
\lambda_a &= -L_a i_a - L_{ab} i_b - L_{ac} i_c + L_{af} i_{fd} + L_{aD} i_D + L_{aQ} i_Q \\
&= -\left(L_{aa0} + L_{aa2}\cos 2\theta\right) i_a + \left(L_{ab0} + L_{ab2}\cos(2\theta + \pi/3)\right) i_b \\
&\quad + \left(L_{ab0} + L_{ab2}\cos(2\theta - \pi/3)\right) i_c + \left(L_{af}\cos\theta\right) i_f \\
&\quad + \left(L_{aD}\cos\theta\right) i_D - \left(L_{aQ}\sin\theta\right) i_Q
\end{aligned}
$$

(2.35)

Similarly,

$$\lambda_b = \left(L_{ab0} + L_{aa2}\cos(2\theta + \pi/3)\right)i_a - \left(L_{aa0} + L_{aa2}\cos 2(\theta - 2\pi/3)\right)i_b$$
$$+\left(L_{ab0} + L_{ab2}\cos(2\theta - \pi)\right)i_c + \left(L_{af}\cos(\theta - 2\pi/3)\right)i_f \tag{2.36}$$
$$+\left(L_{aD}\cos(\theta - 2\pi/3)\right)i_D - \left(L_{aQ}\sin(\theta - 2\pi/3)\right)i_Q$$

and

$$\lambda_c = \left(L_{ab0} + L_{aa2}\cos(2\theta - \pi/3)\right)i_a + \left(L_{ab0} + L_{aa2}\cos(2\theta - \pi)\right)i_b$$
$$-\left(L_{aa0} + L_{aa2}\cos 2(\theta + 2\pi/3)\right)i_c + \left(L_{afd}\cos(\theta + 2\pi/3)\right)i_f \tag{2.37}$$
$$+\left(L_{aD}\cos(\theta + 2\pi/3)\right)i_D - \left(L_{aQ}\sin(\theta + 2\pi/3)\right)i_Q$$

2.3.6. Rotor circuit equations

The rotor circuit voltage equations are

$$e_f = p\lambda_f + r_f i_f \tag{2.38}$$
$$0 = p\lambda_D + r_D i_D \tag{2.39}$$
$$0 = p\lambda_Q + r_Q i_Q \tag{2.40}$$

The rotor circuits see constant permeance because of the cylindrical structure of the stator. Therefore, the self-inductances of rotor circuits and mutual inductances between each other do not vary with rotor position. Only the rotor to stator mutual inductances vary periodically with θ as given by equations (2.32) to (2.34). The rotor circuit flux linkages may be expressed as follows:

$$\lambda_f = L_f i_f + L_{fD} i_D - L_{af}\left(i_a\cos\theta + i_b\cos(\theta - 2\pi/3) + i_c\cos(\theta + 2\pi/3)\right) \tag{2.41}$$
$$\lambda_D = L_{fD} i_f + L_D i_D - L_{aD}\left(i_a\cos\theta + i_b\cos(\theta - 2\pi/3) + i_c\cos(\theta + 2\pi/3)\right) \tag{2.42}$$
$$\lambda_Q = L_Q i_Q + L_{aQ}\left(i_a\sin\theta + i_b\sin(\theta - 2\pi/3) + i_c\sin(\theta + 2\pi/3)\right) \tag{2.43}$$

2.4. The dq0 transformation

The equations (2.13) to (2.15), and equations (2.35) to (2.37) associated with the stator circuits, together with equations (2.38) to (2.40) associated with the rotor circuits, completely describe the electrical performance of a synchronous machine. However, these equations contain inductance terms which vary with angle θ which in turn varies with time. This introduces considerable complexity in solving machine and power system problems.

A much simpler form leading to a clearer physical picture is obtained by appropriate transformation of stator variables. We see from equations (2.41) to (2.43) that stator currents combine into convenient forms in each axis.

This suggests the transformation of the stator currents into new variables as follows:

$$i_d = k_d\left(i_a\cos\theta + i_b\cos(\theta - 2\pi/3) + i_c\cos(\theta + 2\pi/3)\right) \tag{2.44}$$
$$i_q = -k_q\left(i_a\sin\theta + i_b\sin(\theta - 2\pi/3) + i_c\sin(\theta + 2\pi/3)\right) \tag{2.45}$$

The constants k_d and k_q are arbitrary and their values may be chosen to simplify numerical coefficients in performance equations. In most of the literature on synchronous machine theory, k_d and k_q are taken as $2/3$, and this choice will be followed here. An alternative transformation with $k_d = k_q = \sqrt{2/3}$ will be discussed later.

With k_d and k_q equal to $2/3$, for balanced sinusoidal conditions, the peak values of i_d and i_q are equal to the peak value of the stator current as shown below. For the balanced condition:

$$i_a = I_m \sin(\omega_s t)$$
$$i_a = I_m \sin(\omega_s t - 2\pi/3)$$
$$i_a = I_m \sin(\omega_s t + 2\pi/3)$$

Substituting the stator currents in balanced conditions in (2.44). As expected there remains again the traveling wave formulae:

$$i_d = \frac{3}{2} k_d I_m \sin(\omega_s t - \theta) \tag{2.46}$$

For the peak value of i_d to be equal to I_m, k_d should be equal to $2/3$. Again the same applies for equation (2.45):

$$i_q = -\frac{3}{2} k_q I_m \cos(\omega_s t - \theta) \tag{2.47}$$

For an wider analysis of the transformations to obtain (2.46) and (2.47) see the Appendix 3.

Again, $k_q = 2/3$ results in the maximum value of i_q being equal to the peak value of the stator current. To give a complete degree of freedom, a third component must be defined so that the three-phase currents are transformed into three variables. Since the two current components i_d and i_q together produce a field identical to that produced by the original set of phase currents, the third component must produce no space field in the air-gap. Therefore, a convenient third variable is zero sequence current i_0 associated with the symmetrical components:

$$i_0 = \frac{1}{3}(i_a + i_b + i_c)$$

Under balanced conditions $i_a + i_b + i_c = 0$ and therefore $i_0 = 0$. The transformation from the abc phase variables to the $dq0$ variables can be written in the following matrix form:

$$\begin{bmatrix} i_d \\ i_q \\ i_0 \end{bmatrix} = \frac{2}{3} \begin{bmatrix} cos\theta & cos(\theta - 2\pi/3) & cos(\theta + 2\pi/3) \\ -sin\theta & -sin(\theta - 2\pi/3) & -sin(\theta + 2\pi/3) \\ 1/2 & 1/2 & 1/2 \end{bmatrix} \begin{bmatrix} i_a \\ i_b \\ i_c \end{bmatrix} \tag{2.48}$$

For the Per-Unit explanation, the rotor-side bases quantities and the normalizing voltage and flux equations we reference to the Appendix 4.

In the previous section, we have gotten the mathematical description of the synchronous machine working as generator. Now with those equations we will build the bond graph model.

In previous work has been established the bond graph model. Of course, these representations have light differences between them due to the sign convention, and considerations done by the authors.

In order to avoid confusions, we will transform the voltage and flux equations previously obtained to a bond graph model, and considering that the use of reactances X for inductances L or M is based on the rationale that ω_{en} is nearly constant at 1.0 p.u so that, in p.u, $X = \omega L \cong L$.
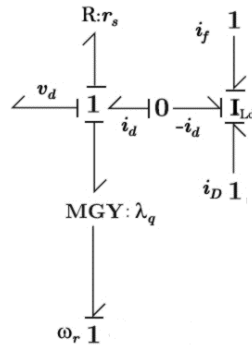
- Field

$$e_f = r_f \, i_f + p\lambda_f$$

$$\lambda_f = \frac{1}{\omega_{en}}\left(X_f \, i_f - X_{md} \, i_d + X_{md} \, i_D \right)$$
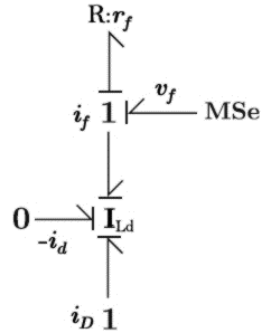
- Direct axis

$$v_d = -r_s \, i_d - \omega_r \lambda_q + p\lambda_d$$

$$\lambda_d = \frac{1}{\omega_{en}}\left(-X_d \, i_d + X_{md} \, i_f + X_{md} \, i_D \right)$$

- Quadrature axis

$$v_q = -r_s \, i_q + \omega_r \lambda_d + p\lambda_q$$

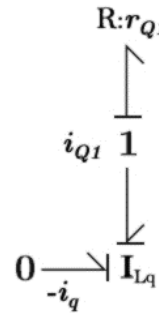$$\lambda_q = \frac{1}{\omega_{en}}\left(-X_q \, i_q + X_{mq} \, i_Q \right)$$
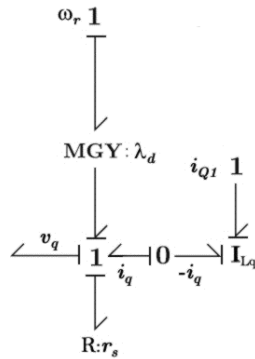
- Damper windings

$$0 = r_D \, i_D + p\lambda_D$$

$$\lambda_D = \frac{1}{\omega_{en}}\left(X_D \, i_D - X_{md} \, i_d + X_{md} \, i_f \right)$$
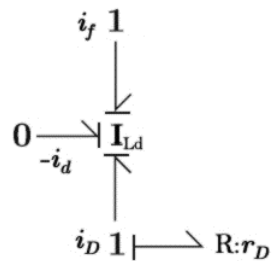
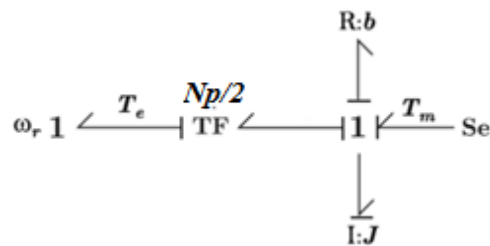$$0 = r_Q\, i_Q + p\lambda_Q$$

$$\lambda_Q = \frac{1}{\omega_{en}}\left(X_Q\, i_Q - X_{mq}\, i_q\right)$$

- Mechanical domain

$$T_e = \frac{N_p}{2}\left(\lambda_d\, i_q - \lambda_q i_d\right)$$

$$J\frac{2}{N_p}\frac{d\omega_r}{dx} = T_m - T_e - T_{f\omega}$$

- Park transformation

$$(\theta_r) = \sqrt{\frac{2}{3}}\begin{bmatrix} \cos\theta_r & \cos(\theta_r - 2\pi/3) & \cos(\theta_r + 2\pi/3) \\ -\sin\theta_r & -\sin(\theta_r - 2\pi/3) & -\sin(\theta_r + 2\pi/3) \end{bmatrix}$$

We now make some observations regarding the nature of the above equations, the equation

$$v_0 = -r_s\, i_0 - X_0\, \tfrac{d}{dt} i_0$$

is not coupled to other equations. Therefore, it can be treated separately. The variables v_0, X_0, and i_0 are known as the zero-sequence variables. The name originally comes from the theory of symmetrical components. These fictitious equations are needed to make the transformation possible when the sum of the three-phase current is not zero, i.e., unbalanced system. Since we are considering balanced systems, to remove this equation is justified.

Finally, the bond graph model of the synchronous machine is shown in Figure 14. For generator convention, the three MS_e associated with the voltages $e_{a,b,c}$ are to be interpreted as sinks or electric loads and the mechanical S_e as the primary mover.
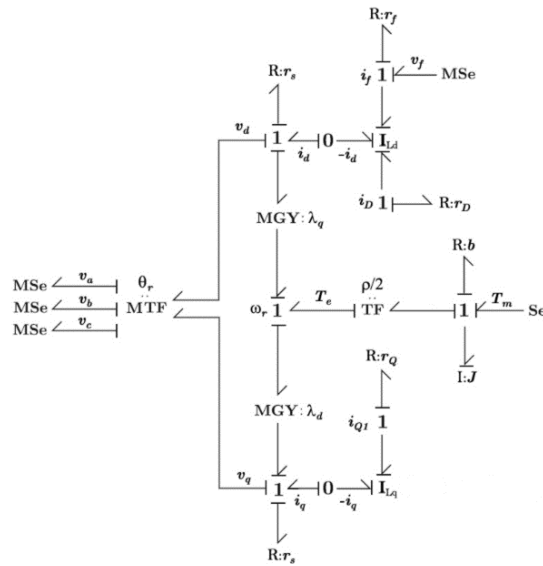
Figure 14: Bond Graph of *n*-pole, 3-phase synchronous machine, generator convention

The flux relationships in the bond graph are defined by the two I-fields, thus

$$
I_{Ld} = \frac{1}{\omega_{en}} \begin{bmatrix} X_d & X_{md} & X_{md} \\ X_{md} & X_f & X_{md} \\ X_{md} & X_{md} & X_D \end{bmatrix}; \qquad I_{Lq} = \frac{1}{\omega_{en}} \begin{bmatrix} X_q & X_{mq} \\ X_{mq} & X_Q \end{bmatrix} \tag{2.49}
$$

3.   Torsional analysis of the power system

Once we have obtained the Bond Graph model of the synchronous generator, we can create a complete system of two generators sharing load. At the same time, we can add diesel engines, clutches and propels in order to complete the marine electric power system as shown in Figure 15.
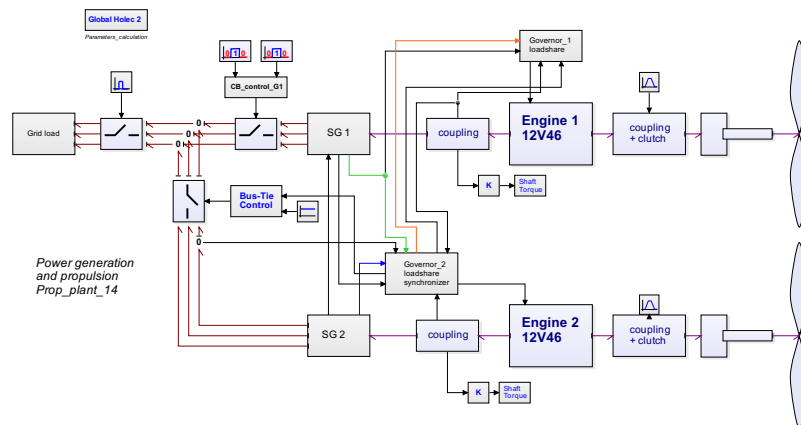

Figure 15: 20-sim iconic simulation model

The system involved is the propulsion and power generation of a dredging vessel consisting of a PS and SB system. Each system, consisting of a Wärtsilä 12V46 engine with on the flywheel side a flexible coupling with clutch, propulsion gearbox and the CPP. See for the diesel model [48]

On the PTO side a flexible coupling and the 6.6 kV 11350 KVA generator. The BG model of the elastic system of the 12-cylinder V engine is handled in [47]. The block on the left-hand upper side contains the parameter calculation for the Park model. So, no need for fiddling with formulae.

To reduce the vibrations induced from the two diesel engines to the ship's structure an elegant solution is to take care that in parallel operation the combustion pulses from diesel 1 not coincide with the combustion pulsus from diesel 2. In this case the generator has 6 pole pares and the diesel generates 3 pulses per revolution:

Combustion sequence: A1B1 – A5B5 – A3B3 – A6B6 – A2B2 – A4B4 it is a for stroke engine, so this take 2 crank shaft revolutions. Between pulse A and pulse B is 45°. So, every 120° there is a combined combustion pulse. So, to ensure that the pulses do not coincide there should be 60° phase difference between the crank shaft of diesel 1 and crank shaft of diesel 2.

The generator has 6 pole pares so every 360°/6 = 60°, these are mechanical degrees, there is zero phase difference and the generators can be switched parallel. 60° mechanical is 360° electrical. From the above it is clear that to ensure that the combustion pulses do not coincide there should be a mechanical angle between the shaft position of generator 1 and generator 2 when from both diesels cylinder A1 is in TDC with a value that gives not an integer when divided by 6. We used $42_m^\circ = 252_e^\circ = 4.3982\ [rad]$. See Appendix 5 with a slightly modified synchronous generator model with the ability to adjust the rotor position to the diesel.

The next simulation outputs demonstrate the synchronizing in the voltage and the shaft torque of the generators.
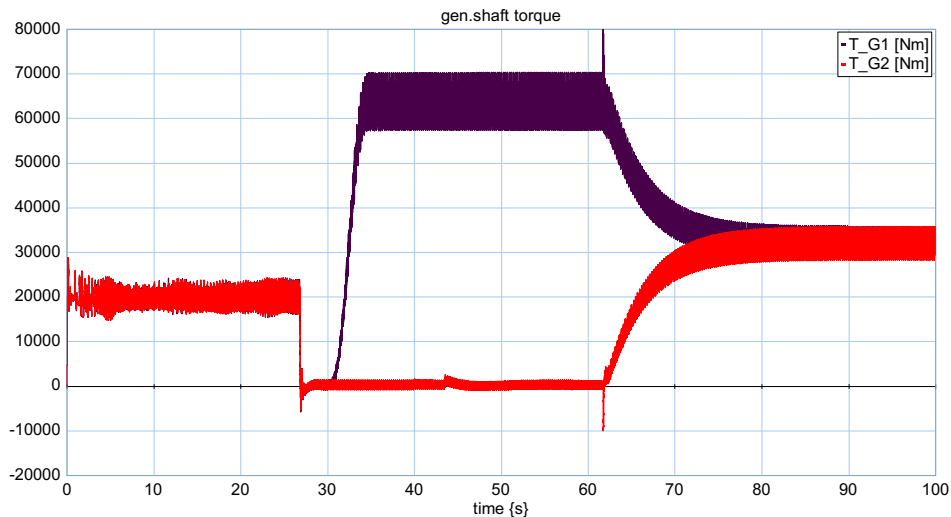

Figure 16: Simulation output of the generator shaft torque: black line gen. 1 and the red line gen. 2

Figure 16 depicts speed-up to nominal (t= 0 to t = 27 sec.) at t = 30 sec. a load step to 3.4 MW on generator 1. At t = 40 sec. the synchronizer is switched on and at t = 43 sec. the phase control is switched on and at phase difference is < 2 [degree] the CB is closed (t = about 62 sec.) and the load sharing starts.
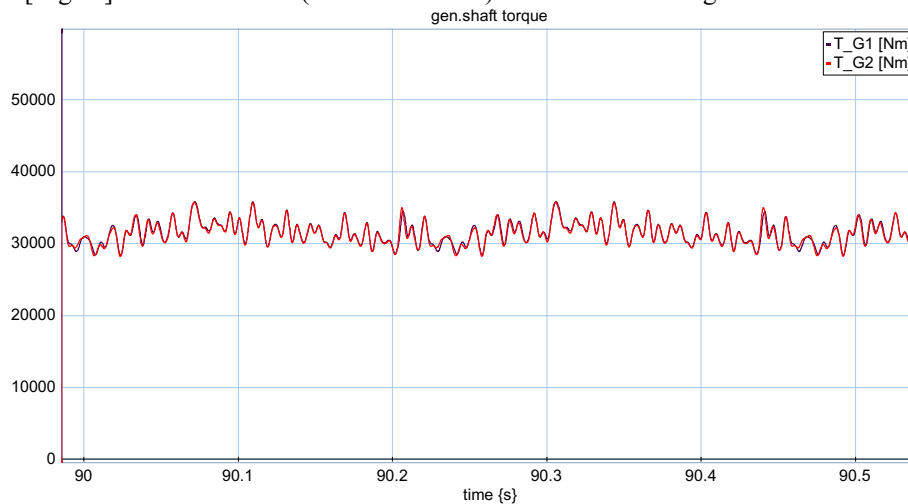

Figure 17: Shaft torque gen 1 (black) line and gen 2 (red line)

The torque pulses coincide. Both generators are mounted equal to the diesel crankshaft.
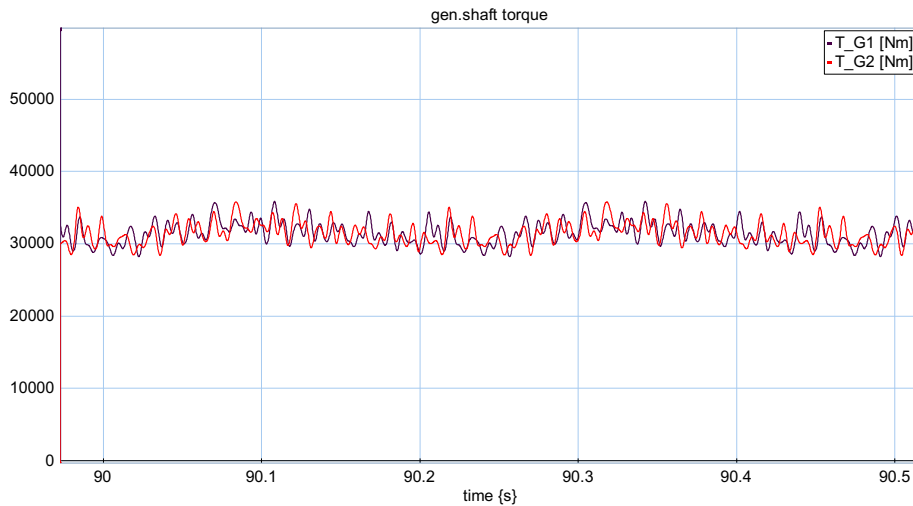
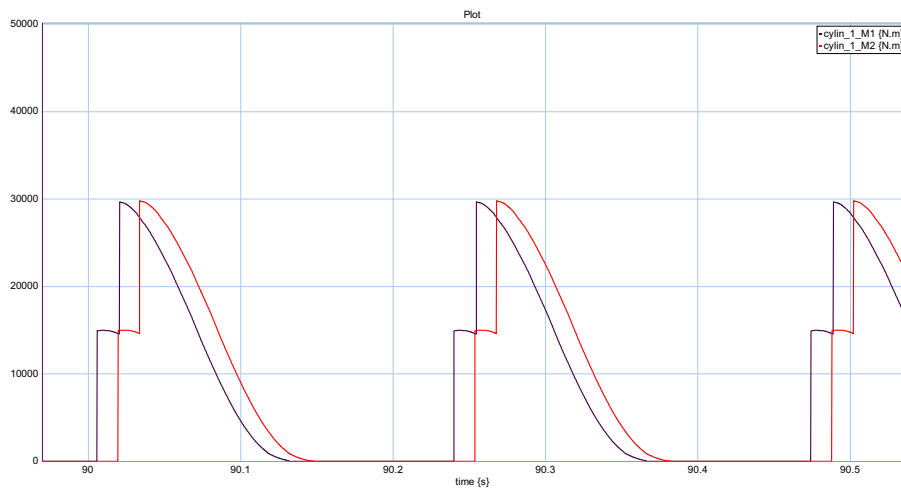Figure 18: The shaft of gen. 2 is now mounted to the crank shaft of diesel 2 as described in previous page.

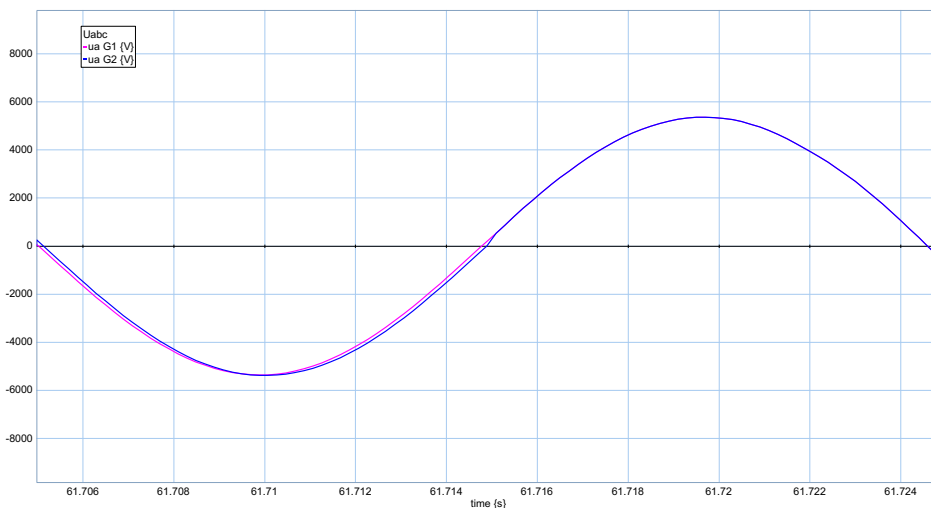Figure 19: The combustion pulses do not coincide now

Figure 20: A plot of the voltage of gen 1 (red line) and gen 2 (blue line) and the current in phase a of gen.2

At phase difference < 2 [degree] the CB is closed and the synchronizing torque, see [47] is pulling gen 2 full in phase with gen 1.

As mentioned in the introduction an attempt was made to model the nasty habit of a rubber element of the elastic coupling between diesel and generator and diesel and propulsion gearbox.

It took some efforts to get a usable model which generate an output comparable with the measurements. The next model is in line what the reader can find in [55] and [56], an explanation is given in the Appendix 8.

When the TVA calculation , two masses and one stiffness [2], depicts that the resonance frequency is more than a factor $\sqrt{2}$ away from the excitation frequencies from the diesel or from the load than a simple stiffness model for the elastic coupling is satisfactory.
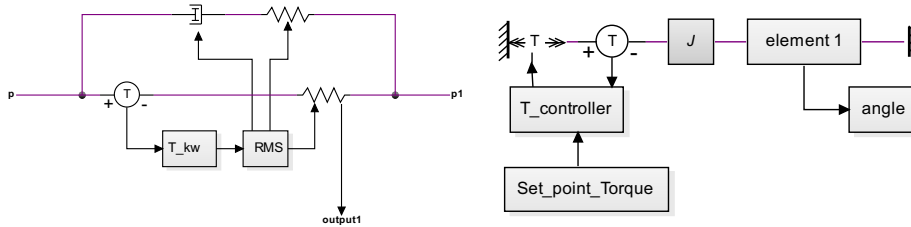

Figure 21: Blockdiagram of the test at Vulkan and the contents of block element 1.
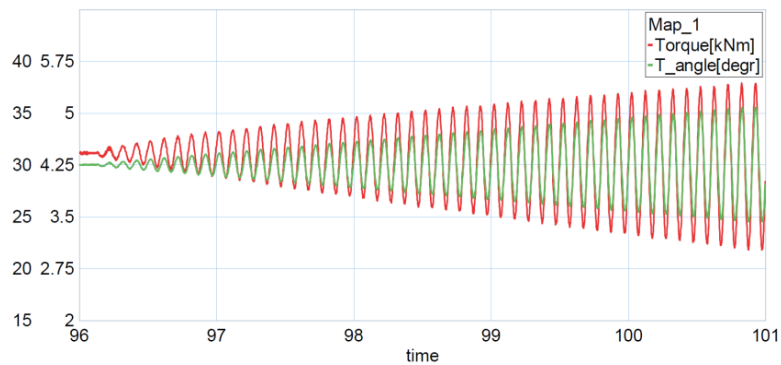

Figure 22: A sample from the measurements at Vulkan, for the Vulkan measurements see the Appendix 8
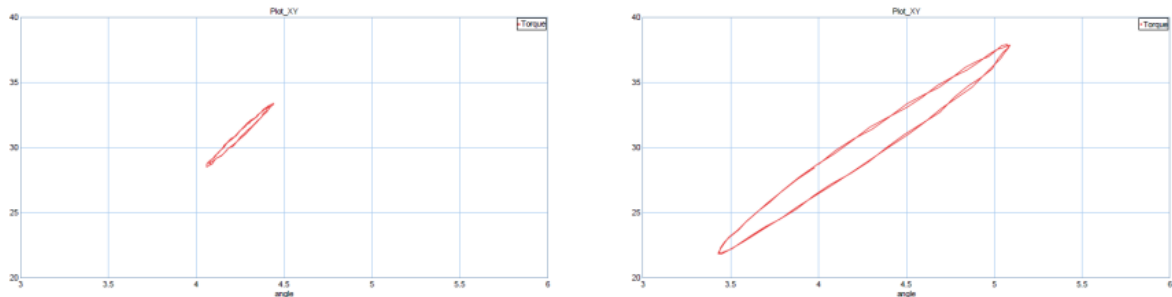

Figure 23: xy-plot torque versus angle from the measurement in Figure 22.

The xy-plot depicts clearly the change in stiffness and damping during changing amplitude of the applied oscillating torque.
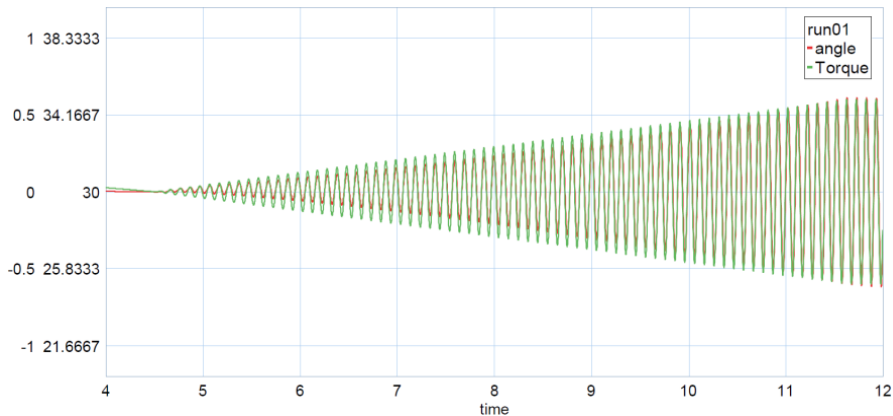
Figure 24: Simulation output

The simulation output is in line with the measurements except that the angle measurement is missing the pre-torque angle. In reverence [55] looks that they were facing the same problem in figure the toque angle is also around the zero. In the Appendix 8 we clarify how we solved this.

Figure 25: xy-plot of the torque versus angle of the model.

4. Conclusions.

The synchronous 3-phase generator appears to be a highly dynamic system. There is a lot of mathematics behind the Bond Graph model but we refer to [6] page 163. In the view of the authors, all relations in electric machine theory (including Gabriel Kron's method of tearing, Park's DQ transformation) just cry out for a Bond Graph representation. So, a desirable representation should replace the complex matrix equations by clear, impressive and beautiful Bond Graph symbols that also help to program the computer. We think the presented model satisfy that.

This paper depicts the power of Bond Graphs in modeling marine engineering systems. The first problem for a control engineer or systems engineer in front of a process to control is to obtain a precise and easily manipulated model with predictions corresponding to the real observations.

The use of 20-sim as a simulation package make life a lot easier because of the ability of direct input of the Bond Graph and 20-sim has the possibility for the engineer to make icons so the model is readable for engineers not familiar with Bond Graphs, and for them there is a large library of iconic models see www.20Sim.com.

The modeling itself is broading the insight and understanding of the system. The most time-consuming part of modeling is to get the right parameters of the system or the systems components. Especially for the synchronous machine there is more data required than the contents of the name plate. It depends largely on knowing the right man on the right place to get the information needed to set up a model that represent the physical system.

And to build a suitable model of an elastic element there is a need for having measurement data as presented in this paper.

Measurements revealed that the simplifications, among other things the generation of the combustion pulses, in the modeling where allowed for this reason finding the resonance frequencies of the system, as mentioned before one looks for relevant analogies, not for complex identities.

References

[1]   Modeling for transient torsional vibration analysis in marine power train systems, Kristine Bruun, Eilif Pedersen and Harald Valland. The Norwegian University of Science and Technology. Department of Marine Technology.

[2]   Mechanical Vibrations Dover, J.P. den Hartog, 1985. ISBN 0-486-64785-4

[3]   Power Systems Analysis, Hadi Saadat

[4]   Bondgraaftechniek (in Dutch), T. Nannenberg, Delta Press, 1987 ISBN 90-6674-1256

[5]   System Dynamics, Dean C. Karnopp, Donand L. Marlolis, Ronald C. Rosenberg, John Wiley. 2000 ISBN 0-471-33301-8

[6]   Simulation by Bond Graphs. Introduction to a Graphical Method, Jean U. Thoma. Springer, 1990 ISBN 3-540-51640-9 (very good for the practical engineer)

[7]   Power System Dynamics and Stability, Jan Machowski, Janus W. Bialek, James R. Bumby. John Wiley & Sons.

[8]   Stabilization of the Electrotromechanical Oscillations of Synchronous Generator. Damir Sumina, Neven Bulic, and Srdan Skok

[9]   Modelling for transient performance simulation of diesel engines using Bond Graphs, Hallvard Engja, ISME 1983, page 321 - 328.

[10]   The Bond graph technique as a powerful modeling tool, Hallvard Engja, International symposium on Advances in Marine Technology, page 471 - 441.

[11]   Vulkan Technical data sheet: RATO-ETD

[12]   Application of Bond graphs for mathematical modelling and simulation of marine, Hallvard Engja, PTMC 2004 papers, pages 11 – engineering systems. Trans IMarEST, Vol 110, part 4 pp 229-239.

[13]   Bond Graphs: A representation for mechatronic systems, P.J. Gawthrop, Mechatronics Vol 1, No. 2 pp 127-156, 1991

[14]   Metamodelling: Bond graphs and dynamic systems, Peter Gawthrop, Lorcan Smith, Prentice Hall ISBN 0-13-489824-9

[15]   Bond Graphs for Engineers, P.C. Breedveld and G. Dauphin-Tanguy: North-Holland 1992.

[16]   Engineering around a hydraulic controlled gearbox, T. Heeringa, PTMC 2004 papers, pages 11 – 36.

[17]   Modelling and Simulation in Thermal and Chemical Engineering, Thoma, B. Ould Bouamama, Springer. ISBN 3-540-66388-6

[18]   On the Modeling and Simulation of Friction, D.A. Haessig, B. Friedland, Transactions of the ASME Vol. 113, September 1991 pages 354 – 362.

[19]   Modelling and control of marine engineering systems, T. Heeringa, PTMC 2006 papers, pages: 225 – 249.

[20]   Stationäres Betriebsverhalten der Synchronmaschine am starren Netz, Prof. Dr.-Ing. Habil. U. Beckert. TU Bergakademie Freiberg, Institut für Elektrotechniek

[21]   Electric Power Systems, B.M. Weedy, John Wiley & Sons.

[22]   Electrische Maschinen, Rolf Fischer, Carl Hanser Verlag

[23]   Elements of Power System Analysis, William D. Stevenson, Jr. McGraw-Hill.

[24]   Graph Modeling of Marine Power Systems, Tom Arne Pedersen, Doctoral thesis at NTNU, 2009

[25]   Alternating Current Machines M. G. Say ELBS/Longman (The AC machines book for the practical engineer).

[26]   Friction Models and Friction Compensation. H. Olsson, K. J. Åström, M. Gäfvert, C. Canudas de Wit, P. Lischinsky.

[27]   Power System Stability and Control, Kundur, P., McGraw-Hill, 1993

[28]   Bond Graph Modelling of Engineering Systems. Wolfgang Borutzky Springer.

[29]   On dynamic properties of rubber isolators. Doctoral Thesis Mattias Sjöberg, ISRN KTH/KT/D--02/39--SE

[30]   The elasticity and related properties of rubbers, (http://iopscience.iop.org/0034-4885/36/7/001)

[31]   Engineering Viscoelasticity. David Roylance, Department of Materials Science and Engineering. MIT Cambridge, October 24, 2001.

[32]   On the modelling of nonlinear elastomeric vibration isolators, Journal of Sound and Vibration (1999) 219(2), 239-253.

[33]   Influence of temperature on characteristics properties of flexible coupling. Jaroslav HOMISIN, Peter KASSAY, Department of Mechanisms. Faculty of Engineering, Technical University Kosice.

[34]   Vulkan Couplings, Explanation of technical data. 08/2016.

[35]   https://tel.archives-ouvertes.fr/tel-00563111/document document in French

[36]   An alternative model for static and dynamic friction in dynamic system simulation. Peter J Breedveld. 1st IFAC-conference on Mechatronic systems, September 18-20, 2000 Darmstad, Germany, Vol 2, pp. 717-722.

[37]   VULKAN Couplings, Explanation of technical data for marine applications and stationary energy production. 08/2016. See: www.vulkan.com

[38] EP-Based Optimisation for Estimation Synchronising and Damping Torque Coefficients. N.A.M. Kamari, I. Musirin, Z.A. Hamid, M.N.A. Rahim, Energy and Power 20123, 2(2): 17-23

[39] Introduction to Physical Systems Modelling with Bond Graphs, Jan F. Broenink. University of Twente.

[40] A Bond Graph Approach for the Modelling and Simulation of a Buck Converter. Rached Zrafi, Sami Ghedira and Kamel Besbes. Journal of Low Power Electronics and Applications.

[41] Modeling & Simulation 2018. Lecture 8. Bond graphs, Claudio Altafini Automatic Control, ISY Linköping University, Sweden

[42] Orthogonal matrix Wikipedia

[43] IEEE Guide for Synchronous generator modeling IEEE Std 1110-2002

[44] IEC 60034-4 Ed.3, Rotating electrical machines. Part 4: methods for determining synchronous machine quantities from tests, in: International Electrotechnical Commission, May 2008.

[45] A two-axis Bond Graph Model of the Dynamics of Synchronous Electrical Machines, Dietrich Sahm, Journal of the Franklin Institute, 302(3):205-218, 1979

[46] Power System Control and Stability, P.M. Anderson, A.A. Fouad, 2nd edition, John Wiley & Sons, Inc., 2003

[47] Torsional Vibration Analysis by Bond Graph Modeling, A practical approach, T. Heeringa INEC 2018

References for modelling elastic elements.

[48] On dynamic properties of rubber isolators. Doctoral Thesis Mattias Sjöberg, ISRN KTH/KT/D--02/39—SE

[49] The elasticity and related properties of rubbers, (http://iopscience.iop.org/0034-48 85/36/7/001)

[50] Engineering Viscoelasticity. David Roylance, Department of Materials Science and Engineering. MIT Cambridge, Oktober 24, 2001.

[51] On the modelling of nonlinear elastomeric vibration isolators, Journal of Sound and Vibration (1999) 219(2), 239-253.

[52] Influence of temperature on characteristics properties of flexible coupling. Jaroslav HOMISIN, Peter KASSAY, Department of Mechanisms. Faculty of Engineering, Technical University Kosice.

[53] Vulkan Couplings, Explanation of technical data. 08/2016

[54] Finite element procedures in modelling the dynamic properties of rubber, Doctoral Thesis by Anders K. Olsson. Lund University Sweden, March 2007.

[55] Modelling of rubber components using estimated parameters. 24th International Symposium on Dynamics of Vehicles on Roads and Tracs IAVSD 2015, Graz, Austria, August 17 – 21 , 2015 (Paper 17.1)

[56] A physically motivated model for filled elastomers including strain rate and amplitude dependency in finite viscoelasticity. International Journal of Plasticity 78 (2016) 223-241

[57] Novel Empirical Model of Rubber Bushing in Automotive Suspension System. Zhang Lijun, Yu Zengliang, Yu Zhuoping. Proceedings of ISMA2010 4259 – 4274.

[58] Dynamic Stiffness and Damping Prediction on Rubber Material Parts, FEA and Experimental Correlation. Zorion Karaeaga Laka . Lea Artibai Ikastetxea S.Coop and London Metropolitan University. PhD – Doctor Europaeus 2016

[59] Chapter 33. Mechanical Properties of Rubber. Ronald J. Schaefer.

[60] Dynamic Torsional Stiffness of Natural Rubber in Shear Couplings under the influence of preload, amplitude frequency, and rotational speed. Mahamudul Hassan and Rick I. Zadoks, Torsional Vibration Symposium Salzburg 2017.

Appendix 1: Review of magnetic circuit equations

The basic calculation method of a magnetic circuit is the same as is used in a basic electrical analysis using Ohm's law. The total magnetic flux Φ (analogous to electric current), magnetomotive force F (analogous to voltage), and magnetic reluctance R (analogous to electrical resistance) are related as shown below:

$$\text{Total magnetic flux } \Phi = \frac{Magnetomotive\ force\ F}{Magnetic\ reluctance\ R}$$

In magnetic circuit calculations, it is more common to use the magnetic permeance P, which is the reciprocal to reluctance R. Using permeance instead of reluctance, the total flux equation is changed as shown below:

$$\text{Total magnetic flux } \Phi = Magnetomotive\ force\ F \cdot Permeance\ P$$

The permeance P is a function of the magnetic circuit length L magnetic circuit cross sectional area A, and the magnetic permeability μ.

$$Permeance\ P = \frac{Permeability\ \mu \cdot Cross\ sectional\ area\ A}{Magnetic\ circuit\ length\ L}$$

Single excited circuit

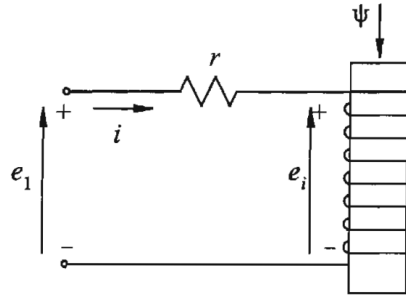We consider first the elementary circuit of Figure 26.

Figure 26: Single-excited magnetic circuit [27].

Comprising a single exciting coil, the coil has N turns and a resistance of r. It is assumed to have a linear flux-mmf relationship. According to Faraday's law, the induced voltage e_i is

$$e_i = \frac{d\Psi}{dt} \tag{A1.1}$$

where Ψ is the instantaneous value of flux linkage. The terminal voltage e_1 is given by

$$e_1 = e_i + ri \tag{A1.2}$$

The flux linkage may be expressed in terms of the inductance L of the circuit:

$$\Psi = Li \tag{A1.3}$$

The inductance, by definition, is equal to flux linkage per unit current. Therefore,

$$L = \frac{\Phi}{i} = N^2 P \tag{A1.4}$$

where P is the permeance of magnetic path, and $\Phi = (MMF)P = NiP$ is the flux.
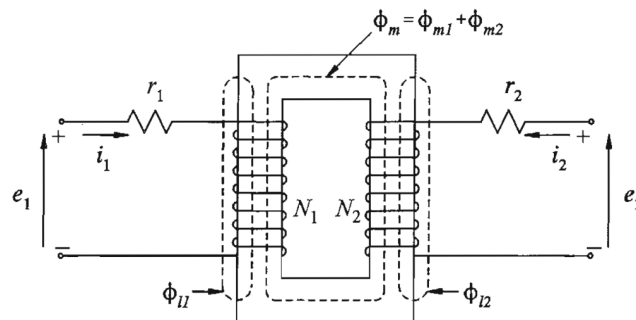
Let us next consider the circuit shown in Figure 27.

Figure 27: Magnetically coupled circuits [27].

Consisting of two magnetically coupled windings. The windings have turns N_1 and N_2, and resistances r_1 and r_2, respectively; the magnetic path is assumed to have linear flux-mmf relationship. The winding currents i_1 and i_2 are considered positive into the windings as shown in the figure. The terminal voltages are

$$e_1 = \frac{d\Psi_1}{dt} + r_1 i_1 \tag{A1.5}$$

$$e_2 = \frac{d\Psi_2}{dt} + r_2 i_2 \tag{A1.6}$$

The magnetic field is determined by currents in both windings. Therefore, Ψ_1 and Ψ_2 are the flux linkages with the respective windings produced by the total effect of both currents. Thus

$$\Psi_1 = N_1 \left(\Phi_{m1} + \Phi_{ml1} \right) + N_1 \Phi_{m2} \tag{A1.7}$$

$$\Psi_2 = N_2 \left(\Phi_{m2} + \Phi_{ml2} \right) + N_2 \Phi_{m1} \tag{A1.8}$$

where

$\Phi_{m1} = $ mutual flux linking both windings due to current in winding 1 acting alone

$\Phi_{l1} = $ leakage flux linking winding 1 only

$\Phi_{m2} = $ mutual flux linking both windings due to current in winding 2 acting alone

$\Phi_{l2} = $ leakage flux linking winding 2 only

The flux linkages can be expressed in terms of self and mutual inductances whose expressions are give below. Accordingly, the self inductances of windings 1 and 2 are:

$$L_{11} = N_1(\Phi_{m1} + \Phi_{l1})/i_1 \qquad \text{or} \qquad L_{11}i_1 = N_1(\Phi_{m1} + \Phi_{l1}) \tag{A1.9}$$

$$L_{22} = N_2(\Phi_{m2} + \Phi_{l2})/i_2 \qquad \text{or} \qquad L_{22}i_2 = N_2(\Phi_{m2} + \Phi_{l2}) \tag{A1.10}$$

or

$$L_{11} = L_{m1} + L_{l1} \tag{A1.11}$$

$$L_{22} = L_{m2} + L_{l2} \tag{A1.12}$$

where L_{m1} and L_{m2} are the magnitizing inductances, and L_{l1} and L_{l2} the leakage inductances of the respective windings.

Mutual inductance between two windings, by definition, is the flux linkage with one winding per unit current in the other winding. Therefore, the mutual inductasnces between windings 1 and 2 are:

$$L_{12} = \frac{N_1 \Phi_{m2}}{i_2} \tag{A1.13}$$

and

$$L_{21} = \frac{N_2 \Phi_{m1}}{i_1} \tag{A1.14}$$

If P is the permeance of the mutual flux path,

$$\Phi_{m1} = N_1 i_1 P \tag{A1.15}$$

$$\Phi_{m2} = N_2 i_2 P \tag{A1.16}$$

From equations (A1.13) to (A1.16), we see that

$$L_{12} = L_{21} = N_1 N_2 P \tag{A1.17}$$

Substitution of equations (A1.9) and (A1.13) in equation (A1.7), equations (A1.10) and (A1.14) in equation (A1.8) gives the following expressions for flux linking windings 1 and 2 in terms of mutual inductances:

$$\Psi_1 = L_{11}i_1 + L_{12}i_2 \tag{A1.18}$$
$$\Psi_2 = L_{21}i_1 + L_{22}i_2 \tag{A1.19}$$

In the above equations, it is important to recognize the relative directions of self and mutual flux linkages by the use of an appropriate algabraic sign for the mutual inductance. The mutual inductance is positive if currents in the two windings produce self and mutual fluxes in the same direction.

Equations (A1.5) and (A1.6) for voltage together with equations (A1.18) and (A1.19) for flux linkage give performance equations of the linear static coupled circuits of Figure 27. In this form of representation, the self and mutual inductances of the windings are used as parameters. As seen from equations (A1.4) and (A1.17), an inductance is directly proportional to the permeance of the associated flux path.

In developing the equations of magnetic circuits in this section, we have not explicitly specified units of system quantities, these equations are valid in any consistent system of units.

Finally, before we turn to the synchrionous machine equations, a comment about notation used is appropriate. In circuit analysis, symbol λ is commonly used to denote flux linkage, whereas in most literature on synchronous machines and power system stability the symbol Ψ is used.

Appendix 2: The traveling wave equation

Let us consider:

$$
\begin{aligned}
MMF_{total} &= MMF_a + MMF_b + MMF_c \\
&= KI_m \left[\cos(\omega_s t)\cos\gamma + \cos(\omega_s t - 2\pi/3)\cos(\gamma - 2\pi/3) + \cos(\omega_s t + 2\pi/3)\cos(\gamma + 2\pi/3) \right]
\end{aligned} \tag{A2.1}
$$

with the help of the trigonometric identity $\cos\alpha\cos\beta = (1/2)\cos(\alpha+\beta) + (1/2)\cos(\alpha-\beta)$ we simplify (A2.1) to:

$$
\begin{aligned}
MMF_{total} &= KI_m \begin{bmatrix} \dfrac{1}{2}\cos(\omega_s t + \gamma) + \dfrac{1}{2}\cos(\omega_s t - \gamma) \\[2mm] +\dfrac{1}{2}\cos(\omega_s t + \gamma - 2\pi/3 - 2\pi/3) + \dfrac{1}{2}\cos(\omega_s t - \gamma - 2\pi/3 + 2\pi/3) \\[2mm] +\dfrac{1}{2}\cos(\omega_s t + \gamma + 2\pi/3 + 2\pi/3) + \dfrac{1}{2}\cos(\omega_s t - \gamma + 2\pi/3 - 2\pi/3) \end{bmatrix} \\[4mm]
&= \frac{1}{2}KI_m \begin{bmatrix} \cos(\omega_s t + \gamma) + \cos(\omega_s t - \gamma) \\[1mm] +\cos(\omega_s t + \gamma - 4\pi/3) + \cos(\omega_s t - \gamma) \\[1mm] +\cos(\omega_s t + \gamma + 4\pi/3) + \cos(\omega_s t - \gamma) \end{bmatrix} \\[4mm]
&= \frac{1}{2}KI_m \left[\cos(\omega_s t + \gamma) + 3\cos(\omega_s t - \gamma) + \cos(\omega_s t + \gamma - 4\pi/3) + \cos(\omega_s t + \gamma + 4\pi/3) \right]
\end{aligned} \tag{A2.2}
$$

If we consider the following substitutions: $\delta = \omega_s t + \gamma$, $\vartheta = -4\pi/3$, and $\rho = 4\pi/3$, then

$$MMF_{total} = \frac{1}{2}KI_m \left[\cos\delta + 3\cos(\omega_s t - \gamma) + \cos(\delta + \vartheta) + \cos(\delta + \rho) \right] \tag{A2.3}$$

If we substitute the trigonometric identity $\cos(\alpha + \beta) = \cos\alpha\cos\beta - \sin\alpha\sin\beta$ in (A2.3):

$$\begin{aligned}
MMF_{total} &= \frac{1}{2}KI_m\left[\cos\delta + 3\cos\left(\omega_s t - \gamma\right) + \cos\left(\delta + \vartheta\right) + \cos\left(\delta + \rho\right)\right] \\
&= \frac{1}{2}KI_m\begin{bmatrix} \cos\delta + 3\cos\left(\omega_s t - \gamma\right) + \cos\delta\cos\vartheta \\ -\sin\delta\sin\vartheta + \cos\delta cos\rho - \sin\delta\sin\rho \end{bmatrix} \\
&= \frac{1}{2}KI_m\left[\cos\delta + 3\cos\left(\omega_s t - \gamma\right) - \frac{1}{2}\cos\delta + \frac{\sqrt{3}}{2}\sin\delta - \frac{1}{2}\cos\delta - \frac{\sqrt{3}}{2}sin\delta\right] \\
&= \frac{3}{2}KI_m\cos\left(\omega_s t - \gamma\right)
\end{aligned}$$
(A2.4)

As we can see in (A2.4) what remains is a mmf with a function of time and a function of place:

Appendix 3: Stator mutual inductances.

The mutual inductance between any two stator winding also exhibits a second harmonic variation because of the rotor shape (salient rotor). It is always negative and has the greatest absolute value when the north and south poles are equidistant from the centers of the two windings concerned. For example, L_{ab} has maximum absolute value when $\theta = \pi/6$ or $\theta = 5\pi/6$.

The mutual inductance L_{ab} can be found by evaluating the air-gap flux ϕ_{gab} linking phase-b when only phase-a is excited. As we wish to find the flux linking phase-b due to mmf of phase-a, θ is replaced by $\theta - 2\pi/3$ in equation (2.21).

$$\begin{aligned}
\phi_{gba} &= \phi_{gad}\cos\left(\theta - 2\pi/3\right) - \phi_{gaq}\sin\left(\theta - 2\pi/3\right) \\
&= \left(N_a i_a cos\theta\right)\cos\left(\theta - 2\pi/3\right)P_d - \left(-N_a i_a \sin\theta\right)\sin\left(\theta - 2\pi/3\right)P_q \\
&= N_a i_a\left[\cos\theta\cos\left(\theta - 2\pi/3\right)P_d + \sin\theta\sin\left(\theta - 2\pi/3\right)P_q\right]
\end{aligned}$$
(A3.1)

with the help of:

$$\cos\alpha\cos\beta = \frac{1}{2}\cos\left(\alpha+\beta\right) + \frac{1}{2}\cos\left(\alpha-\beta\right) \quad \text{and} \quad \sin\alpha\sin\beta = \frac{1}{2}\cos\left(\alpha-\beta\right) - \frac{1}{2}\cos\left(\alpha+\beta\right)$$

We get:

$$\begin{aligned}
\phi_{gba} &= N_a i_a\begin{bmatrix} \frac{1}{2}\cos\left(\theta+\theta-2\pi/3\right)P_d + \frac{1}{2}\cos\left(\theta-\theta+2\pi/3\right)P_d \\ -\frac{1}{2}\cos\left(\theta+\theta-2\pi/3\right)P_q + \frac{1}{2}\cos\left(\theta-\theta+2\pi/3\right)P_q \end{bmatrix} \\
&= \frac{1}{2}N_a i_a\left[\cos\left(2\theta-2\pi/3\right)P_d + \cos\left(2\pi/3\right)P_d - \cos\left(2\theta-2\pi/3\right)P_q + \cos\left(2\pi/3\right)P_q\right] \\
&= \frac{1}{2}N_a i_a\left[\cos\left(2\theta-2\pi/3\right)P_d - \frac{1}{2}P_d - \cos\left(2\theta-2\pi/3\right)P_q - \frac{1}{2}P_q\right] \\
&= \frac{1}{2}N_a i_a\left[-\frac{1}{2}\left(P_d+P_q\right) + \left(P_d-P_q\right)\cos\left(2\theta-2\pi/3\right)\right] \\
&= N_a i_a\left[-\frac{1}{4}\left(P_d+P_q\right) + \frac{1}{2}\left(P_d-P_q\right)\cos\left(2\theta-2\pi/3\right)\right]
\end{aligned}$$
(A3.2)

The mutual inductance between phases-a and -b due to the air-gap flux is

$$L_{ab} = \frac{N_a \phi_{gba}}{i_a}$$

$$= -\frac{1}{2} L_{g0} + L_{ab2} \cos(2\theta - 2\pi/3)$$

(A3.3)

where L_{g0} has the same meaning as in expression for self-inductance L_a given by equation (2.24). There is a very small amount of mutual flux around the ends of the windings which does not cross the air-gap. With this flux included, the mutual inductance between phases-a and -b can be written as

$$L_{ab} = L_{ba} = -L_{ab0} + L_{ab2} \cos(2\theta - 2\pi/3)$$

$$= -L_{ab0} - L_{ab2} \cos(2\theta + \pi/3)$$

(A3.4)

Similarly,

$$L_{bc} = L_{cb} = -L_{ab0} - L_{ab2} \cos(2\theta - \pi)$$

(A3.5)

$$L_{ca} = L_{ac} = -L_{ab0} - L_{ab2} \cos(2\theta - \pi/3)$$

(A3.6)

From the above equations, it can be readily seen that $L_{ab2} = L_{aa2}$. This is to be expected since the same variation in permeance produces the second harmonic terms in self and mutual inductances, it can also be seen that L_{ab0} is nearly equal to $L_{aa2}/2$.

The variation of mutual inductance between phases a and b as a function of θ is illustrated in Figure 28.
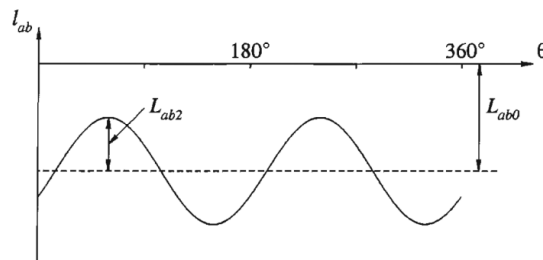

Figure 28: Variation of mutual inductance between stator windings.

For the balanced condition:

$$i_a = I_m \sin \omega_s t$$

$$i_b = I_m \sin(\omega_s t - 2\pi/3)$$

$$i_c = I_m \sin(\omega_s t + 2\pi/3)$$

Substituting i_a, i_b, and i_c in equation (2.44) gives:

$$i_d = k_d \left[I_m \sin(\omega_s t) \cos\theta + I_m \sin(\omega_s t - 2\pi/3) \cos(\theta - 2\pi/3) + I_m \sin(\omega_s t + 2\pi/3) \cos(\theta + 2\pi/3) \right]$$

with the help of:

$$\sin\alpha \cos\beta = \frac{1}{2}\sin(a+\beta) + \frac{1}{2}\cos(\alpha - \beta)$$

we get:

$$i_d = I_m k_d \begin{bmatrix} \dfrac{1}{2}\sin\left(\omega_s t + \theta\right) + \dfrac{1}{2}\sin\left(\omega_s t - \theta\right) \\ + \dfrac{1}{2}\sin\left(\omega_s t - 2\pi/3 + \theta - 2\pi/3\right) + \dfrac{1}{2}\sin\left(\omega_s t - 2\pi/3 - \theta + 2\pi/3\right) \\ + \dfrac{1}{2}\sin\left(\omega_s t + 2\pi/3 + \theta + 2\pi/3\right) + \dfrac{1}{2}\sin\left(\omega_s t + 2\pi/3 - \theta - 2\pi/3\right) \end{bmatrix}$$

$$= \frac{1}{2} I_m k_d \left[3\sin\left(\omega_s t - \theta\right) + \sin\left(\omega_s t + \theta\right) + \sin\left(\omega_s t - 4\pi/3 + \theta\right) + \sin\left(\omega_s t + 4\pi/3 + \theta\right) \right]$$

(A3.7)

Propose: $\delta = \omega_s t + \theta$, $\vartheta = 4\pi/3$ on the last three terms:

$$\sin\delta + \sin\left(\delta - \vartheta\right) + \sin\left(\delta + \vartheta\right)$$

With the help of formulae $\sin\left(\alpha \pm \beta\right) = \sin\alpha\cos\beta \pm \cos\alpha\sin\beta$

$$= \sin\delta + \sin\delta\cos\vartheta - \cos\delta\sin\vartheta + \sin\delta\cos\vartheta + \cos\delta\sin\vartheta$$

$$= \sin\delta - \frac{1}{2}\sin\delta + \frac{\sqrt{3}}{2}\sin\delta - \frac{1}{2}\sin\delta - \frac{\sqrt{3}}{2}\sin\delta$$

$$= 0$$

So as expected there remains again the traveling wave formulae:

$$i_d = \frac{3}{2} k_d I_m \sin\left(\omega_s t - \theta\right)$$

(A3.8)

For the peak value of i_d to be equal to I_m, k_d should be equal to $2/3$. Again, the same applies for equation (2.47),

$$i_q = -\frac{3}{2} k_q I_m \cos\left(\omega_s t - \theta\right)$$

(A3.9)

Again, $K_q = 2/3$ results in the maximum value of i_q being equal to the peak value of the stator current. Simple example of transformation. e.g. an inductor with N turns, we want to represent that with an "equivalent" coil with 1 turn. We have

$$V_{old} = L\frac{di_{old}}{dt} + i_{old}R$$

If we go from N turns to 1 turn, we instinctively know that we must decrease the volts by N and increase the current by N. To keep the equation right we must adjust the impedance by $N*N$.

$$i_{old} = \frac{i_{new}}{N}$$

$$V_{new} = \frac{V_{old}}{N}$$

$$V_{new} = \frac{L}{N^2}\frac{di_{new}}{dt} + \frac{R}{N^2}i_{new}$$

In matrix notation:

$$\left[i_{old}\right] = \left[C\right]\left[i_{new}\right]$$

The system needs to be the "same" after transformation: keep complex power constant – so called power invariance

Appendix 4: Per-unit model

For this section, we highly recommend pages 92-97 in [46]. We want to normalize the voltage equations, that is, we desire to express them in per-unit. Some advantages of doing so are:
- The per-unit system offers computational simplicity by eliminating units and expressing system quantities as dimensionless ratios
- The numerical values of currents and voltages are related to their rated values irrespective of machine size.
- Impedances, when given on the machine base, lie on a relatively narrow range so that errors can be easily detected.

There are several different possible normalization schemes. Note that machine manufacturers, when expressing their machine data in per-unit, may use a different system that does not satisfy the power invariance property of Park transformation (they use Park's original transformation).

The choice made by [46] satisfies the above criteria; in addition, it ensures that the numerical values of the per-unit impedances are the same as those provided by manufacturers using their system of normalization.

However, if all base quantities are arbitrarily selected, equations describing physical laws will have to be modified in the new base system. In general equations describing physical laws in an arbitrarily selected per unit system are complex. To avoid this complication it is necessary to select the base quantities in such a way that physical laws are expressed with the same equations in terms of per unitized quantities and a physical system of units such as the metric system for example.

In multicircui networks, which are not interconnected, but magnetically coupled (as the synchronous generator), there is a certain degree of freedom in selecting the base quantities for the per-unit system. One should exercise this freedom towards simplification of the equations and possible physical interpretation of mathematical models. This stated objective can be defined as follows:
- The form of the system voltage equations should be exactly the same whether the equations are expressed in p.u or metric system units.
- The form of the system power equations must be invariant (same in p.u or actual metric units).
- The per-unit system should be selected in such a way that mutual inductances can be represented with T-equivalent circuits, after per-unitization.

Stator-side bases quantities

We choose the following stator base quantities.

$V_{n\phi} = V_B = V_R$ the stator nominal (or base or rated) line-neutral voltage, rms
$S_n = S_B = S_R$ the stator nominal (or base or rated) per-phase power, volt-amps
$\omega_{en} = \omega_B = \omega_R$ the generator nominal (or base or rated) speed, in electrical rad/sec

Notice that the words nominal, base, and rated refers to the same variable, we will use the word nominal. We now develop the relations for the various base quantities.

$I_n = \dfrac{S_n}{V_{n\phi}}$ the stator nominal current, amps

$\lambda_n = \dfrac{V_{\phi n}}{\omega_{en}}$ the stator nominal magnetic flux, webers

$L_n = \dfrac{\lambda_n}{I_n}$ the stator nominal inductance, henrys

$R_n = \dfrac{V_{n\phi}}{I_n}$ the stator nominal resistance, ohms

$t_n = \dfrac{1}{\omega_{en}}$ the stator nominal time, seconds

To normalize any quantity, it is divided by the base quantity of the same dimension. For example, for currents we write

$$i_{(pu)} = \frac{i\{A\}}{I_n\{A\}}\{p.u\} \tag{A4.1}$$

where we use the subscript (*pu*) to indicate per-unit values. Later, when there is no danger of ambiguity in the notation, this subscript is omitted.

Rotor-side bases quantities

The choice made here for the rotor base quantity is based on the concept of *equal mutual flux linkages.* That is, we select the base currents for the three rotor-side windings f, D, and Q to produce the same mutual flux in the air gap as produced by the stator-side nominal current I_n flowing in the corresponding fictitious d-axis (q-axis) coil.

If we denote the magnetizing inductances as:

$$
\begin{aligned}
L_{md} &= L_d - L_{ls}; \quad L_{mq} = L_q - L_{ls} \\
L_{mf} &= L_f - L_{lf}; \quad L_{mQ} = L_Q - L_{lQ} \\
L_{mD} &= L_D - L_{lD}
\end{aligned}
\tag{A4.2}
$$

and equate the mutual flux linkages in each winding,

$$
\begin{aligned}
\lambda_{md} &= L_{md} I_n = Km_{sf} I_{fn} = Km_{sD} I_{Dn} \ \{Wb\} \\
\lambda_{mf} &= Km_{sf} I_n = L_{mf} I_{fn} = Km_{fD} I_{Dn} \ \{Wb\} \\
\lambda_{mD} &= Km_{sD} I_n = Km_{fD} I_{fn} = L_{mD} I_{Dn} \ \{Wb\} \\
\lambda_{mq} &= L_{mq} I_n = Km_{sQ} I_{Qn} \ \{Wb\} \\
\lambda_{mQ} &= Km_{sQ} I_n = L_{mQ} I_{Qn} \ \{Wb\}
\end{aligned}
\tag{A4.3}
$$

where
I_{fn} is the field nominal current, amps

I_{Dn} is the D damping winding nominal current, amps

I_{Qn} is the Q damping winding nominal current, amps

Then we can show that

$$
\begin{aligned}
L_{md} I_n^2 &= L_{mf} I_{fn}^2 = L_{mD} I_{Dn}^2 = Km_{sf} I_{fn} I_n = Km_{sD} I_{Dn} I_n = Km_{fD} I_{Dn} I_{fn} \\
L_{mq} I_n^2 &= Km_{sQ} I_{Qn} \ I_n = L_{mQ} I_{Qn}^2
\end{aligned}
\tag{A4.4}
$$

and this is the fundamental constrain among base currents. From (A4.4) and the requirements for equal power, $S_n = S_{nf} = S_{nD} = S_{nQ}$, we compute

$$
\begin{aligned}
K_f &\triangleq \frac{V_{fn}}{V_{n\phi}} = \frac{I_n}{I_{fn}} = \sqrt{\frac{L_{mf}}{L_{md}}} = \frac{Km_{sf}}{L_{md}} = \frac{L_{mf}}{Km_{sf}} = \frac{Km_{fD}}{Km_{sD}} \\
K_D &\triangleq \frac{V_{Dn}}{V_{n\phi}} = \frac{I_n}{I_{Dn}} = \sqrt{\frac{L_{mD}}{L_{md}}} = \frac{Km_{sD}}{L_{md}} = \frac{L_{mD}}{Km_{sD}} = \frac{Km_{fD}}{Km_{sf}} \\
K_Q &\triangleq \frac{V_{Qn}}{V_{n\phi}} = \frac{I_n}{I_{Qn}} = \sqrt{\frac{L_{mQ}}{L_{mq}}} = \frac{Km_{sQ}}{L_{mq}} = \frac{L_{mQ}}{Km_{sQ}}
\end{aligned}
\tag{A4.5}
$$

The basic constraints permit us to compute

$$
\begin{aligned}
R_{fn} &= K_f^2 R_n \ \{\Omega\}; \quad L_{fn} = K_f^2 L_n \ \{H\} \\
R_{Dn} &= K_D^2 R_n \ \{\Omega\}; \quad L_{Dn} = K_D^2 L_n \ \{H\} \\
R_{Qn} &= K_Q^2 R_n \ \{\Omega\} \quad L_{Qn} = K_Q^2 L_n \ \{H\}
\end{aligned}
\tag{A4.6}
$$

and the base mutual must be the geometric mean of the base self-inductances:

$$m_{fn} = K_f L_n \{H\}; \quad m_{Qn} = K_Q L_n \{H\}$$
$$m_{Dn} = K_D L_n \{H\}; \quad m_{fDn} = K_f K_D L_n \{H\}$$

(A4.7)

Normalizing the voltage, and flux equations

Having chosen appropriate base values, we may normalize the machine voltage equations, for the *d*-axis we have:

$$v_d = -r_s\, i_d - \omega_r\left(-L_q\, i_q + Km_{sQ}\, i_Q\right) + \tfrac{d}{dt}\left(-L_d\, i_d + Km_{sf}\, i_f + Km_{sD}\, i_D\right)$$

(A4.8)

Regarding to the concept of per-unit value from (A4.1), then (A4.8) is converted into:

$$V_{n\phi} v_{d(pu)} = -r_s\, I_n i_{d(pu)} - \omega_{en}\omega_{r(pu)}\left(-L_q\, I_n i_{q(pu)} + Km_{sQ}\, I_{Qn} i_{Q(pu)}\right)$$
$$+ \tfrac{d}{dt}\left(-L_d I_n\, i_{d(pu)} + Km_{sf}\, I_{fn} i_{f(pu)} + Km_{sD}\, I_{Dn} i_{D(pu)}\right)$$
$$v_{d(pu)} = -r_s \frac{I_n}{V_{n\phi}} i_{d(pu)} - \omega_{en}\omega_{r(pu)}\left(-L_q \frac{I_n}{V_{n\phi}} i_{q(pu)} + Km_{sQ}\frac{I_{Qn}}{V_{n\phi}} i_{Q(pu)}\right)$$
$$+ \frac{d}{dt}\left(-\frac{L_d}{\omega_{en}}\frac{\omega_{en}I_n}{V_{n\phi}} i_{d(pu)} + \frac{Km_{sf}}{\omega_{en}}\frac{\omega_{en}I_{fn}}{V_{n\phi}} i_{f(pu)} + \frac{Km_{sD}}{\omega_{en}}\frac{\omega_{en}I_{Dn}}{V_{n\phi}} i_{D(pu)}\right)$$

(A4.9)

The time may be normalize, nevertheless, is not common to do it, so we will not normalize it. Incorporating the stator base values, we rewrite (A4.9) as

$$v_{d(pu)} = -\frac{r_s}{R_n} i_{d(pu)} - \omega_{r(pu)}\left(-\frac{L_q}{L_n} i_{q(pu)} + Km_{sQ}\frac{\omega_{en}I_{Qn}}{V_{n\phi}} i_{Q(pu)}\right)$$
$$+ \frac{d}{dt}\left(-\frac{L_d}{L_n\omega_{en}} i_{d(pu)} + \frac{Km_{sf}}{\omega_{en}}\frac{\omega_{en}I_{fn}}{V_{n\phi}} i_{f(pu)} + \frac{Km_{sD}}{\omega_{en}}\frac{\omega_{en}I_{Dn}}{V_{n\phi}} i_{D(pu)}\right)$$

(A4.10)

Taking into account normalizing procedure we can denote as follows:

$$r_{s(pu)} = \frac{r_s}{R_n}; \quad L_{q(pu)} = \frac{L_q}{L_n}; \quad L_{d(pu)} = \frac{L_d}{L_n}; \quad L_{md(pu)} = Km_{sD}I_{Dn}\frac{\omega_{en}}{V_{n\phi}} = L_{md}I_n\frac{\omega_{en}}{V_{n\phi}} = \frac{L_{md}}{L_n}$$
$$L_{md(pu)} = Km_{sf}I_{fn}\frac{\omega_{en}}{V_{n\phi}} = L_{md}I_n\frac{\omega_{en}}{V_{n\phi}} = \frac{L_{md}}{L_n}; \quad L_{mq(pu)} = Km_{sQ}I_{Qn}\frac{\omega_{en}}{V_{n\phi}} = L_{mq}I_n\frac{\omega_{en}}{V_{n\phi}} = \frac{L_{mq}}{L_n}$$

(A4.11)

Using notation from (A4.11), the *d*-axis equation (A4.10) may be rewritten with all values in p.u except time as,

$$v_{d(pu)} = -r_{s(pu)}\, i_{d(pu)} - \frac{\omega_r}{\omega_{en}}\left(-L_{q(pu)} i_{q(pu)} + L_{mq(pu)} i_{Q(pu)}\right)$$
$$+ \frac{1}{\omega_{en}}\frac{d}{dt}\left(-L_{d(pu)}\, i_{d(pu)} + L_{md(pu)} i_{f(pu)} + L_{md(pu)} i_{D(pu)}\right)$$

(A4.11)

By doing similar procedure for all the voltage equations, and flux equations. Now, we can obtain the per-unit equations of the synchronous generator:

$$v_{d(pu)} = -r_{s(pu)} i_{d(pu)} - \omega_r \lambda_{q(pu)} + \tfrac{d}{dt} \lambda_{d(pu)}$$

$$v_{q(pu)} = -r_{s(pu)} i_{q(pu)} + \omega_r \lambda_{d(pu)} + \tfrac{d}{dt} \lambda_{q(pu)}$$

$$v_{0(pu)} = -r_{s(pu)} i_{0(pu)} + \tfrac{d}{dt} \lambda_{0(pu)}$$

$$v_{f(pu)} = r_{f(pu)} i_{f(pu)} + \tfrac{d}{dt} \lambda_{f(pu)}$$

$$0 = r_{D(pu)} i_{D(pu)} + \tfrac{d}{dt} \lambda_{D(pu)}$$

$$0 = r_{Q(pu)} i_{Q(pu)} + \tfrac{d}{dt} \lambda_{Q(pu)}$$

(A4.12)

and,

$$\lambda_{d(pu)} = \tfrac{1}{\omega_{en}} \left(-L_{d(pu)} i_{d(pu)} + L_{md(pu)} i_{f(pu)} + L_{md(pu)} i_{D(pu)} \right)$$

$$\lambda_{q(pu)} = \tfrac{1}{\omega_{en}} \left(-L_{q(pu)} i_{q(pu)} + L_{mq(pu)} i_{Q(pu)} \right)$$

$$\lambda_{0(pu)} = \tfrac{1}{\omega_{en}} \left(-L_{0(pu)} i_{0(pu)} \right)$$

$$\lambda_{f(pu)} = \tfrac{1}{\omega_{en}} \left(L_{f(pu)} i_{f(pu)} - L_{md(pu)} i_{d(pu)} + L_{md(pu)} i_{D(pu)} \right)$$

$$\lambda_{D(pu)} = \tfrac{1}{\omega_{en}} \left(L_{D(pu)} i_{D(pu)} - L_{md(pu)} i_{d(pu)} + L_{md(pu)} i_{f(pu)} \right)$$

$$\lambda_{Q(pu)} = \tfrac{1}{\omega_{en}} \left(L_{Q(pu)} i_{Q(pu)} - L_{mq(pu)} i_{q(pu)} \right)$$

(A4.13)

where,

$$L_{d(pu)} = L_{md(pu)} + L_{ls(pu)}; \quad L_{q(pu)} = L_{mq(pu)} + L_{ls(pu)}$$

$$L_{f(pu)} = L_{md(pu)} + L_{lf(pu)}; \quad L_{Q(pu)} = L_{mq(pu)} + L_{lQ(pu)}$$

$$L_{D(pu)} = L_{md(pu)} + L_{lD(pu)}$$

(A4.14)

From this point, we will drop the subscript (*pu*) since all the values are in per-unit. Finally, the T-equivalent circuit of the synchronous generator is show in Figure 29.
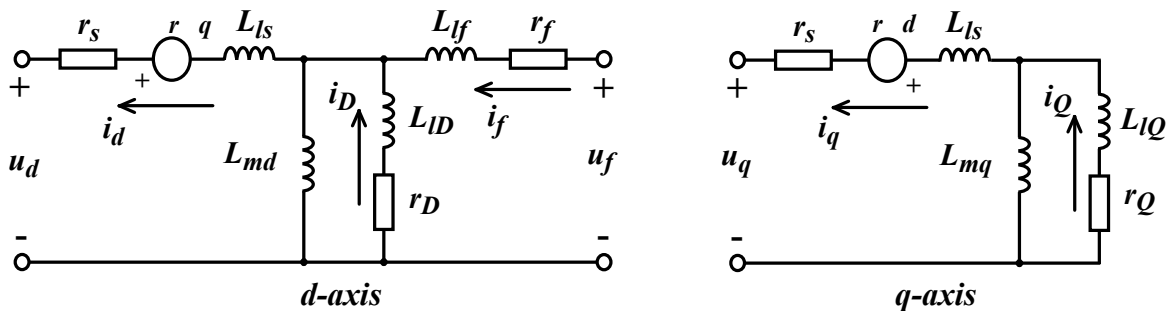
Figure 29: Synchronous generator equivalent circuit after Park transformation

As we can notice the voltage equations did not change, the only difference lies in the flux equations (we have now a division by the nominal electrical speed) because we did not normalize the time.

Normalization of the swing equation

The normalize swing equation is:

$$\frac{2H}{\omega_{en}} \frac{d\omega_r}{dt} = T_{m(pu)} - T_{e(pu)} = T_{a(pu)}$$

(A4.15)

where:

H is the coefficient of normalized inertia, in seconds

$T_{m(pu)}$ is the mechanical torque in p.u

$T_{e(pu)}$ is the electromechanical torque in p.u

For more details of this normalization, we suggest the page 15-16 and 103-105 in [46]. Since the connection between our machine and other machines is in SI values, this torque equation will not be used. It is just presented as information. For an extensive explanation of the swing equation see the INEC 2018 paper [47].

Appendix 5: Simulation model Synchronous generator as used in the simulations.
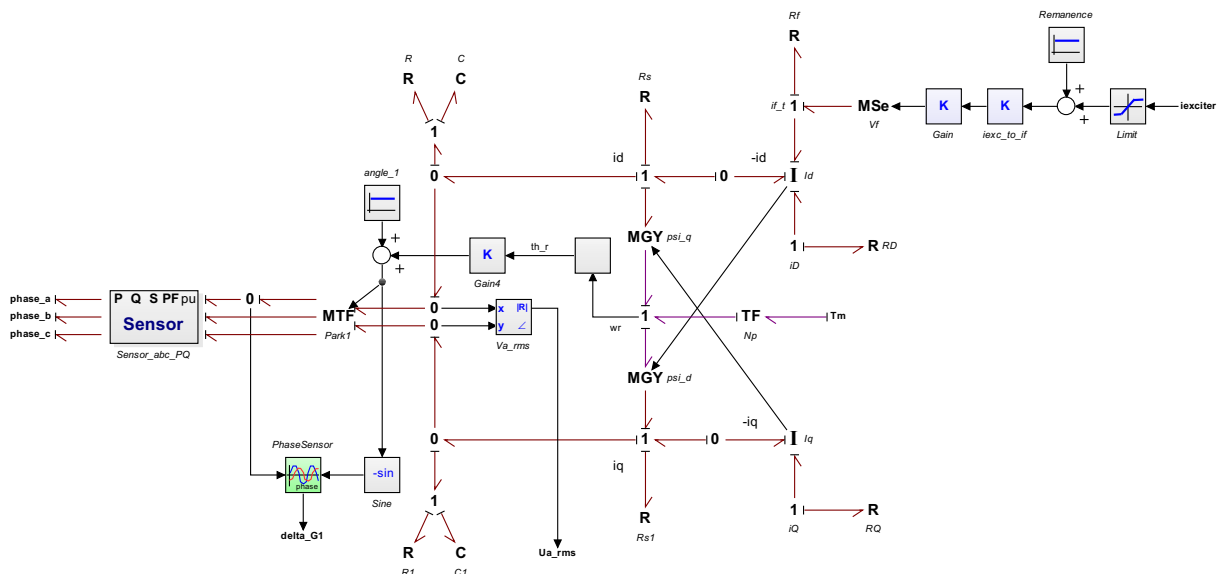
Figure 30: BG synchronous generator model with sensors and shaft positioning.

To reduce diesel induced vibrations to the ship structure is to synchronize the diesels in such a way that the combustion pulses do not coincide. That can be accomplished by connecting the generators in a special way to the diesel crankshaft.

To positioning the rotor poles to the diesel crankshaft the block angle_1, and the block Gain4 are added. The angle_1 block contains the 20-sim command: *output = input mod twopi*, that means that every revolution 2π rad the output is zero and with the value in the block angle_1 we can add an angle value that the generator shaft position to the diesel crankshaft differs from the other generator shaft to the diesel crankshaft.

Figure 31: Mark on the generator shaft indicating a *N*-pole position.

To get this mark on the generator shaft requires a mention in the purchase specification and a check during the FAT and to get each generator mounted in the right position to the diesel requires some attention.

The block PhaseSensor determines the load angle of the generator, and the other sensor block determines the angle between the phase voltage and the phase current also known as power factor or PF of the generator.

Appendix 6: Governor
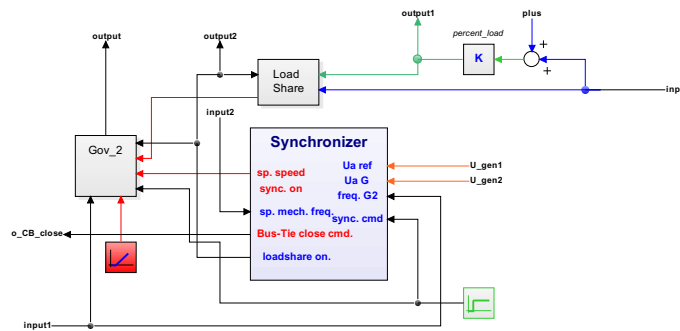
Figure 32: Inside the Governor 2 block.

First an introduction in governing (ship's) diesel engines.
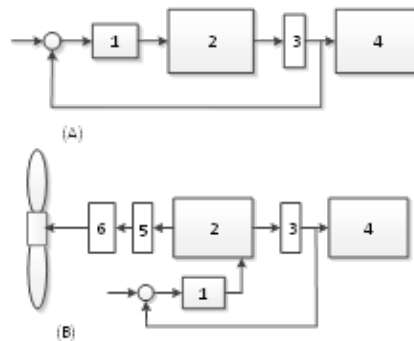
Figure 33: Basic block diagram diesel speed governing, (A) diesel-generator set, (B) ship's propulsion + ship's electrical power generation.

1. speed governor + actuator fuel rack
2. main engine
3. flexible coupling
4. synchronous generator
5. flexible coupling + clutch
6. propulsion gearbox

In general the inertia of the rotor of the synchronous generator is more than the inertia of the diesel crankshaft + flywheel there for the main speed sensor is mounted after the flexible coupling (the angle of rotation is more constant after the flexible coupling) , the back-up speed sensor is from the flywheel.

A proper speed control of a ship's diesel is not an easy task, input block 2 is fuel and output are revolutions. The process gain of a diesel (fuel – revolutions) is not a linear one, the process gain in no load condition of the diesel is high and the process gain in full load condition of the diesel is low. So, a "normal" PID controller cannot handle this task in a proper way. In the early days of the mechanical governor the gain adaption was performed by a nonlinear linkage between governor output shaft and fuel pump linkage (see figure 28 below).

Low gain in no load and high gain at full diesel load
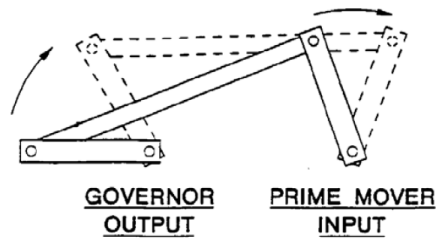
Figure 4-2. Non-Linear Fuel Control

Figure 34: Self-explaining, copied from Woodward documentation (Woodward Manual 26260)

In the nowadays electronic governors this is handled (the nonlinear gain) by software code. Sometimes there is a wish (for a pump drive or a ship's propeller drive) to control the output torque of the diesel and because the process gain is than a linear one , this task is more easy than speed control. Figure 28 depicts the fuel rack versus torque of a Wärtsilä 12V38 engine during commissioning at the Wärtsilä factory in Turku.

In the author's view torque control for the mentioned purposes is not an optimal one , when the pump or propeller starts cavitating the required torque drop's so the controller will increase the diesel revolutions so this will not result in a stable situation.
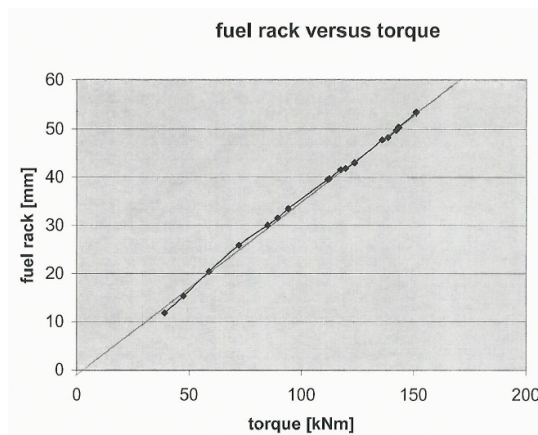
Figure 35: Torque versus fuel rack Wärtsilä 12V38 engine.
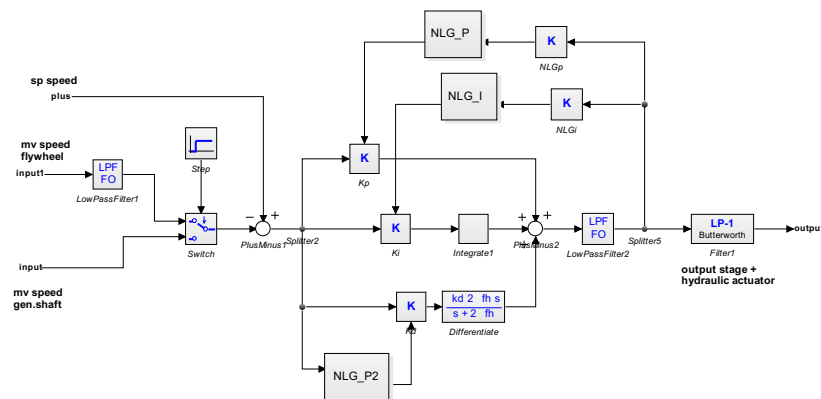
Figure 36: Simplified model for simulations of the Viking 25 governor.

As depicted this is a simplified model, normally the governor has much more variable gains as there are: error dependable gain (small error low gain big error high gain), speed dependable gain, error dependable integration time and error dependable differentiation gain: low error small differentiation action high error no differential action. In the model here is only load dependable gain and load dependable integration time and error dependable derivation time (big error no derivation, small error some derivation) . This model satisfied in the simulations.

The modern diesel is now a common rail engine and this engine is much better to control, today necessary to comply with the exhaust emission rules, the controller output is direct input to the fuel injector.

As depicted in figure 5 the diesel speed can be taken from the flywheel or from the generator shaft. Normally the measured speed is taken from the generator shaft because of the bigger inertia of the generator rotor the speed is more equal than measured from the flywheel.

Also it is clear from figure 1 that the setpoint speed (the red lines) is generated at three places from a ramp up generator for starting the diesel , from the synchronizer and after synchronization from the load share block.

Appendix 7: The synchronizer explained.
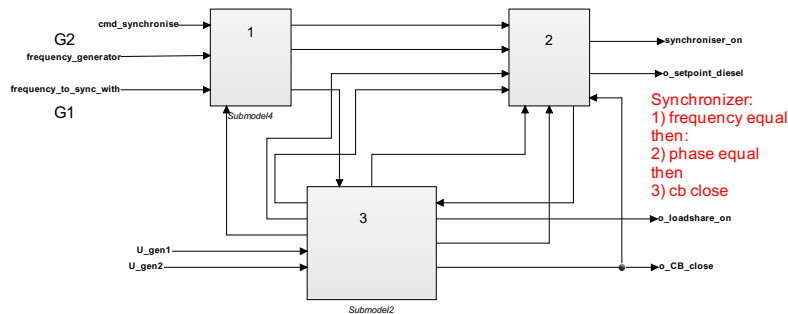
Figure 37: Block diagram of the synchronizer
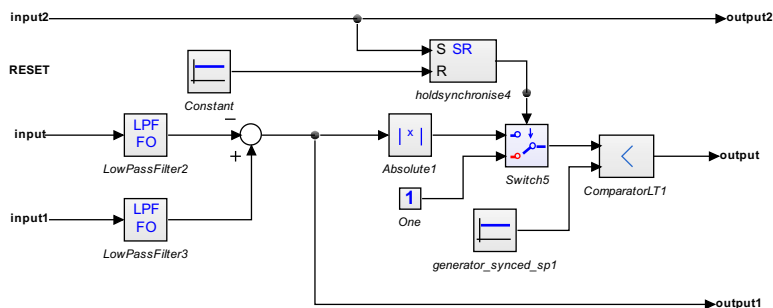
Figure 38: Inside block 1.

Input2 is command synchronizer on, input is frequency generator 1, and input1 frequency generator 2. Output is true if frequency generator 1 = frequency generator 2, and output1 is the frequency error or difference between frequency gen. 1 and frequency gen. 2
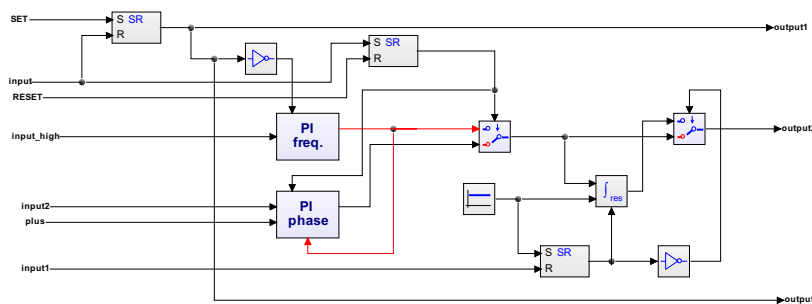
Figure 39: Inside block 2.

For reasons of simplicity this is an analogue synchronizer (most synchronizers are working with a speed up pulse and a speed down pulse for easy interfacing with the diesel speed controller), the block PI freq. is the frequency controller and the block PI phase is the phase controller. The red line from the output PI freq. block is the tracking signal for the PI phase block to ensure a bumble switch over after frequency gen. 2 = frequency gen. 1. Output2 is the speed setpoint to the diesel of generator 2. After the command CB close (generated from the block: phase = equal in block 3) this output is fixed by the tracking integrator of the speed setpoint.
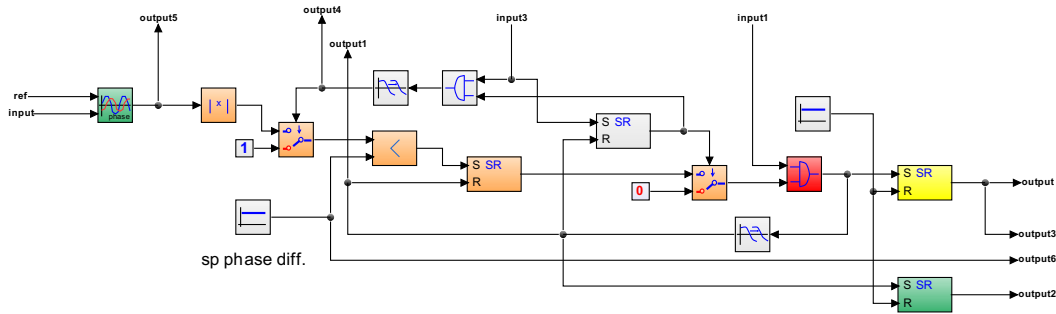
Figure 40: Inside block 3.

This block generates the CB close command, from the green block (a phase comparator) through the orange blocks and the yellow set reset block. The output of the phase comparator is also via output 5 to the phase controller in block 2 see Figure 38.

Appendix 8: Introduction in modelling elasticity.

We start to depict a recording of the measurements by the author during a commissioning at the premises of Vulkan. The modelling of the flexible coupling element is based on these measurements. There is a lot of literature available to model this highly nonlinear piece of equipment but searching in that literature gives no practical usable models, so the model here presented is measurements based. The literature review demonstrates the need of measurement results to derive the parameters of advanced rubber components models [55].
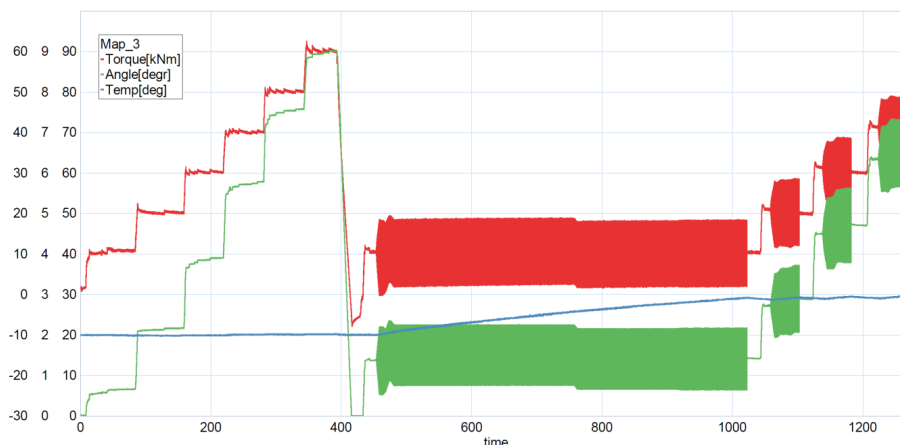
Figure 41: Measurement of the dynamic properties of an elastic element under test at the Vulkan premises.

The plots in Figure 41 are:
- Red: applied torque, scale -30 to 70 kNm.
- Green: deflection angle, scale: 0 to 10 degrees.
- Blue: temperature elastic element, scale: 0 – 100 degrees.

and x-axis is the time in seconds.

Static test is determined in steps of the applied torque of 10 kNm. The dynamic properties are determined by measuring its response to a sinusoidally varying strain, the element is first warmed up by an applied pre torque of 10 kNm and super imposed on the static torque an oscillating torque with an amplitude of 10 kNm with a frequency of 10 Hz. After heating up of the element till 30º the dynamic test starts at 20, 30, and 40 kNm pre-torque
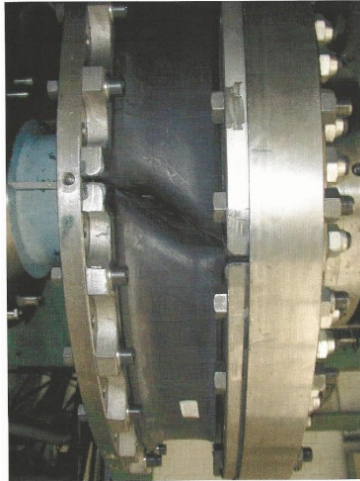
Figure 42: Picture from the test at Vulkan, elastic element under torque

The "Torque angle" or deflection angle is clearly visible, the green line of the measurements.

Dynamic properties of unfilled elastomers: linear viscoelastic materials in cyclic loads.

The applied sinusoidal strain and the resultant stress are plotted as a function of time or phase angle in Figure 43. The maximum elastic and viscous stress, and the elastic and viscous modulus values are calculated using simple trigonometry.
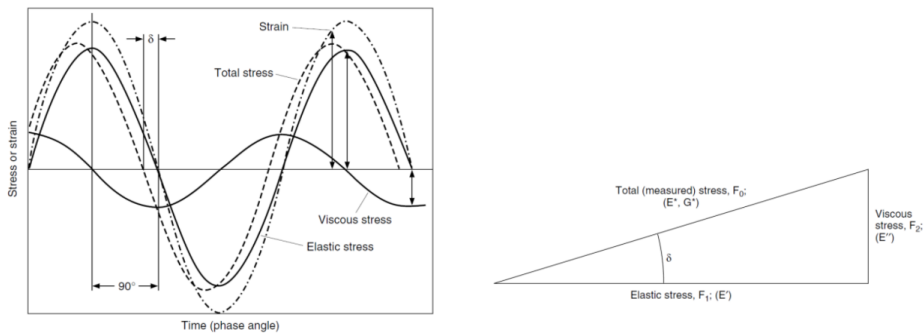

Figure 43: Stress of strain vs phase angle.

Measured at Vulkan a nonlinear elastic element, total stress and angle δ, δ appears to be about 10.5°. The following mathematical approximations are based on the linear viscoelastic theory. The strain varies sinusoidally with time as:

$$\varepsilon = \varepsilon_0 \sin \omega t \qquad (A8.1)$$

where ε_0 is the strain amplitude, the green line, the measured torque angle. The stress σ, the red line, is described by:

$$\sigma = \sigma_0 \sin(\omega t + \delta) \qquad (A8.2)$$

where δ is the phase lag. If (A8.2) is expanded, it can be rewritten as :

$$\sigma = \sigma_0 \omega t \cos \delta + \sigma_0 \omega t \sin \delta \qquad (A8.3)$$

From expression (A8.3), the stress can be considered consisting of 2 components as seen in Figure 43

- $\sigma_0 \cos \delta$: in phase with the strain, proportional to $\sin \omega t$, and

- $\sigma_0 \sin \delta$: $\pi/2$ out of phase with the strain, proportional to $\cos \omega t$

with reverence to Figure 43 we rewrite (A8.3):

$$\sigma = \varepsilon_0 E' \sin \omega t + \varepsilon_0 E'' \cos \omega t \qquad \text{or} \qquad \frac{\sigma}{\varepsilon_0} = E' \sin \omega t + E' \cos \omega t \qquad (A8.4)$$

The dynamic properties can be decomposed in a storage modules E' and loss modules E'' see Figure 44 or equivalently, as complex modulus $E*$ and phase angle δ

$$E' = \frac{\sigma_0}{\varepsilon_0} \cos \delta \qquad (A8.5)$$

$$E'' = \frac{\sigma_0}{\varepsilon_0} \sin \delta \qquad (A8.6)$$

$$E* = \sqrt{(E')^2 + (E'')^2} = \frac{\sigma_0}{\varepsilon_0} \qquad (A8.7)$$

and the phase lag,

$$tan\delta = \frac{E''}{E'} \qquad (A8.8)$$

According to equation (A8.7), the dynamic modulus is the ratio of the peak values of stress σ_0 and strain ε_0. In fact, if strain and stress cycles are sinusoidal, the slope of the axis is defined as the complex modulus $E*$ see again Figure 44 and the xy-plot of the measurement in Figure 45, and the hysteresis area takes the form of an elliptical loop. The elliptical hysteresis loop is associated with the dissipated energy. The E' is the real part complex modulus. It is known as storage modulus because it defines the energy stored in the element produced by the load strain.

Likewise, E'' is called the imaginary part of the complex modulus $E*$. It is called loss modulus since it describes the dissipation of energy, which is evident when calculating the energy per cycle U_c, see annex 11-C of [58].
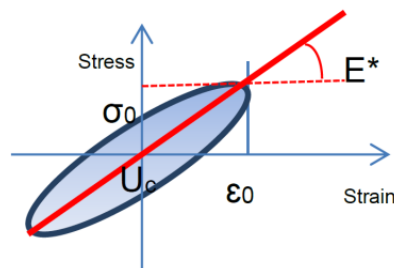

Figure 44: Linear viscoelastic hysteresis loop for harmonic excitation.

$$U_c = \frac{\omega \varepsilon_0^2}{2} E'' \frac{2\pi}{\omega}$$
$$= \pi E'' \varepsilon_0^{\ 2} \qquad (A8.9)$$

This energy is rerptresented by the area of the elliptic hysteresisd loop. If the integral of U_c is evaluated for a quator of a cycles, instead of the entire cycle, the first term gives the maximum stored elastc energy W_c.

$$W_c = \frac{1}{2} E' \varepsilon_0^{\ 2} \qquad (A8.10)$$

If equation (A8.5) is replaced in equation (A8.10)

$$W_c = \frac{1}{2} \sigma_0 \varepsilon_0 \cos \delta \qquad (A8.11)$$

where W_c is ther maximum stored elastic energy, which is independent from the frequency. From these energy expressions, we can deduce that:

$$E' = \frac{2W_c}{\varepsilon_0^{\ 2}} \qquad \text{and} \qquad E'' = \frac{U_c}{\pi\varepsilon_0^{\ 2}}$$

As it is explained above, the damping is the energy loss per cycle and is warming up the element as is depicted in the measurement Figure 41.

As the system is non linear the mentioned hysteresis loop distorts and becomes parallel shaped see the measurement in Figure 46. The dynamic beheaviour of filled elastomers is not linear and this effect is observed in the hysteresis loop. Thes nonlinearities are produced because of the nonlinear elasticity of rubber and the filler structure breakdown and reforming, This filler structure modification produces a decrease of the dynamic modulus induced by the amplitude increasing as depicted in Figure 45. See ref. [58] for an extensive explanation of the fenomenon.
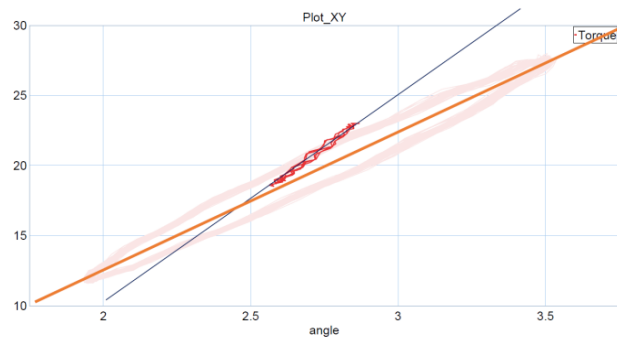
Figure 45: The hysteresis loop from harmonic excitation, this xy-plot is from the measurement at Vulkan.

Nonlinear behavior

Low oscillating torque amplitude high dynamic stiffness, high amplitude oscillating torque lower dynamic stiffness. For an extensive explanation we refer to the reference list.
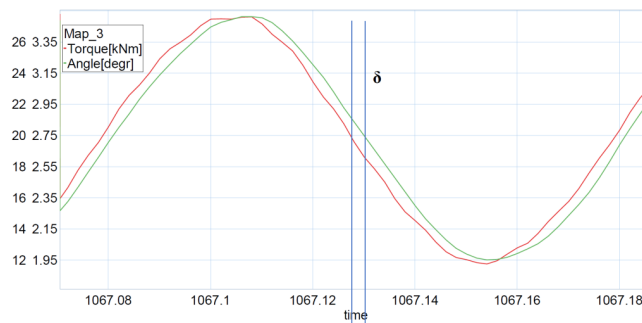

Figure 46: A graph of the sinusoidal strain and resultant stress, from the measurements depicted in Figure 41.

The oscillating applied torque to the element (the red line) lags slightly behind δ the measure of the stress (the green line). This phase shift between stress and strain exists because that part of energy input is not recovered at the end of the cycle. Some of the energy input is stored and recovered in each cycle and some is dissipated as heat, see the measurement of the warming up of the element in Figure 41. Materials whose behavior exhibits such characteristics are called viscoelastic. The phase is a measure of the damping, and thus, also a measure of hysteresis.

Modelling elasticity.

In [54] and [55] some interesting block diagrams are presented and where build with the use of available icons from the 20-sim library and fiddling with the parameters gave results which approximate the measurements of Vulkan and the author.
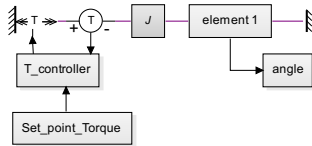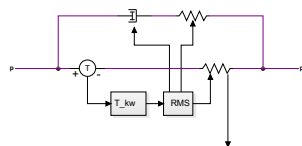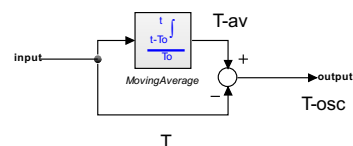
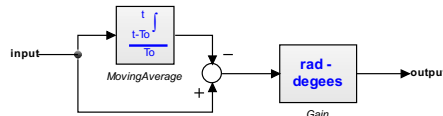Figure 47

Figure 48

Figure 49

Figure 50

Figure 47 depicts the test configuration at VULKAN see the picture at Figure 42, the elastic element is subject to a torque from an hydraulic torque actuator controlled by a torque controller wich is able to apply a pre torque and superimposed to the pre torque an oscilating torque see Figure 41.

Figure 48 is the elastic element an adjustable stiffness and parallel to the stiffness a Maxwell element, see ref [49] with an adjustable damper and adjustable stiffness. The vadjusting parameters are derived from the amplitude of the ocsillating torque generated in the T_kw block. The oscillating torque amplitude is derive as follows: we subtract the "DC" value of the applied torque from the real torque and that gives us the osillating torque value see Figure 49. The RMS block determine the DC value of the oscillating torque and us used to get the adjusting parameters for the stiffness and the Maxwel element.

To get a comparable measurement of the torque angle (see the picture in Figure 42) we have to be creative, also here we deleted the "DC" component or offset in the torque angle measurement and multyplied the value with 57.2958 to get the value in degrees. In [56] there are also figures with a similar simulation output unfortunately a block diagram for a comparison of the model is missing.
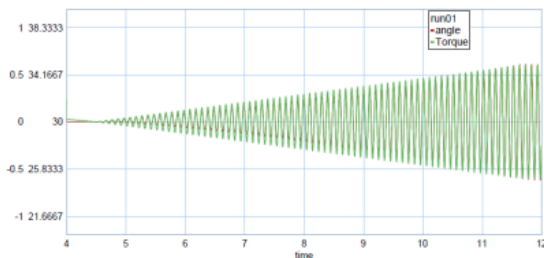

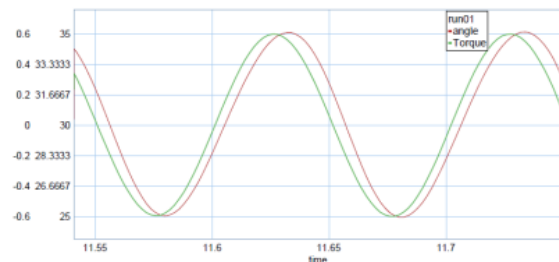Figure 51: Simulation output at a pre-torque of 30 kNm
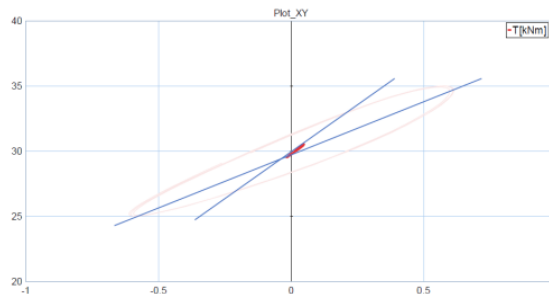

Figure 52: Zoom in of Figure 51.

Figure 53: xy-plot of the applied torque and the torque angle.

The above plot clearly depicts the properties of the elastic element, changing stiffness with increasing amplitude of the applied oscilating torque.